Computers in Biology and Medicine 145 (2022) 105417

Contents lists available at ScienceDirect

Computers in Biology and Medicine

journal homepage: www.elsevier.com/locate/compbiomed

A new active contraction model for the myocardium using a modified hill model

Debao Guan [a], Hao Gao [a,*], Li Cai [b], Xiaoyu Luo [a]

[a] School of Mathematics and Statistics, University of Glasgow, UK
[b] School of Mathematics and Statistics, Northwestern Polytechnical University, Xi'an, China

ARTICLE INFO

Keywords:
Myocardial contraction
Active strain
Hill model
Length-dependence
Force-velocity
Personalized cardiac modelling

ABSTRACT

This study develops a new hybrid active contraction model for myocardial dynamics abstracted from sarcomere by combining the phenomenologically active-stress based Hill model and the micro-structurally motivated active strain approach. This new model consists of a passive branch and a parallel active branch that consists of a serial passive element for active tension transmission and a contractile unit for active tension development. This rheology represents an additive decomposition of the total stress into a passive and active response. The active stress is formulated following the active strain approach based on the sliding filament theory by multiplicatively decomposing the stretch of the contractile element into a fictitious and an active part. The length-dependence and force-velocity are further incorporated in the active strain. We estimate the passive stiffness of the serial passive element using literature data, which is 250 kPa, then the active stress is computed from the serial passive element in the active branch because of its force transmission structure. This one-dimensional contraction model is further generalized to three dimensions for modelling myocardial dynamics. Our results demonstrate that the proposed active contraction model has a high descriptive capability for various experiments, including both isometric and isotonic contraction compared to existing active strain approaches. We also show that it can simulate physiologically accurate cardiac dynamics in humans. The excellent agreement with experimental data and a local sensitivity study highlight the importance of length-dependence and force-velocity in the active strain approach. Our results further show that there exists a tight interaction between the length-dependence and force-velocity relationships. This new hybrid model serves as a step forward in personalized cardiac modelling using an active-strain based contraction model and has the potential to understand the multi-scale coupling in active contraction according to the sliding filament theory.

1. Introduction

Mathematical modelling of cardiac biomechanics has gained wide popularity and success towards the emerge of precision medicine in cardiology, the digital twin of heart [1]. It not only deepens the mechanistic understanding of cardiac function from the cellular level to the tissue/organ level, but also provides novel biomarkers for improved patient care and decision-making [2,3]. Many challenges still exist in the modelling of the myocardium despite decades of efforts being made from both the experimental and modelling communities, and far from being resolved thoroughly [4]. One essential component of cardiac models is the mathematical formulation of the mechanical properties of cardiac tissue, including both passive and active responses.

The contraction of the myocardium is a very complex and synergistic multi-physics/scale process [5]. In literature, approaches to modelling active contraction can be broadly grouped into three categories: active stress, active strain, and hybrid approaches, see [6] for a historical review on cardiac mechanics. As for the first one, the passive stress is often derived from certain strain energy functions (SEF), and an additive active stress tensor [7–9] is included to account for myocardial contraction. The active stress is widely used in personalized cardiac modelling because of its relatively easy implementation and abundant experimental data for parameter calibration because of the additively separated passive and active stress tensors [10–12]. However, it is difficult to formulate SEFs for active contraction due to the complex electrical-chemical-mechanical reactions in active force generation. Instead, active stress is often modelled as a set of ordinary differential equations [9,13].

* Corresponding author.
E-mail address: hao.gao@glasgow.ac.uk (H. Gao).

https://doi.org/10.1016/j.compbiomed.2022.105417
Received 29 December 2021; Received in revised form 11 February 2022; Accepted 21 February 2022
Available online 24 March 2022

Coupling two stress tensors from different concepts in the active stress approach can lead to issues of mathematical convexity [14]. To overcome this, the active strain approach has been developed based on the theories of plasticity, tissue growth and morphogenesis. Kondaurov and Nikitin [15] firstly proposed this framework, further developed by Taber [16] and others [17–20]. The key concept of the active strain approach is the multiplicative decomposition of the deformation gradient tensor $\mathbf{F} = \mathbf{F}_e\mathbf{F}_a$ with $\mathbf{F}_a$ the active strain that stores no elastic energy, which can be fictitiously imagined as plastic distortion of the soft tissue. $\mathbf{F}_a$ may be formulated via prescribed myocardial contraction behaviour. The elastic deformation $\mathbf{F}_e$ accounts for the elastic energy and preserves the compatibility of the soft tissue. Finally, the passive SEF with respect to $\mathbf{F}_e$ can be used to derive the total myocardial stress [19,20]. In the active strain approach, the active and passive stresses are inseparable in general, and thus a SEF is not needed for the active stress but indirectly determined by the passive SEF [20].

A third approach is the hybrid approach [21], which is inspired by the classic Hill model [22] which consists of two nonlinear springs and one contractile element. The Hill model, though considered to be a phenomenological model, still informs today's studies on muscle contraction because of its capability of accurately simulating muscle force generation under various excitation conditions at cellular and tissue levels, myocardial contraction included [13,21]. Interested readers may refer to [6,23] for more details. In the hybrid approach, same as the active stress approach, the total stress is the summation of the active and passive stresses, in which the passive stress is derived from a SEF with respect to the total deformation gradient tensor $\mathbf{F}$. While the active stress is derived from an additive active SEF with respect to $\mathbf{F}_e$ that is determined by $\mathbf{F}\,\mathbf{F}_a^{-1}$ following the active strain approach, and $\mathbf{F}_a$ is defined in a similar way as in the active strain approach. This hybrid approach preserves the advantage of mathematical convexity from the active strain approach whilst separates active and passive contributions to facilitate model calibration.

Active stress approach is rather phenomenological, suffering from the convexity issue [14], while active strain approach is micro-structurally motivated and depends on the local distortions. The multiplicative decomposition of deformation gradient tensor signifies the sequential order between the active distortion and the elastic deformation. In the active strain approach or the hybrid approach, various assumptions have been made to prescribe active strain tensor $\mathbf{F}_a$, such as the transversely isotropic model with $\det \mathbf{F}_a = 1$ [19,24], while it has difficulty in producing physiologically correct ejection fraction and wall thickening. The transversely isotropic model with contraction only occurring along myofibres [14] could overcome the above limitations by not restricting $\det \mathbf{F}_a = 1$. Alternatively, the orthotropic model [25] could predict the physiological wall thickening in systole by defining different contractility along the myofibre and sheet directions based on the assumption that myofibre contraction induces the expansion along the sheet direction by maintaining $\det \mathbf{F}_a = 1$. One essential component in the active strain approach is to describe the contractile function along each axial direction. The temporal evolution of these contractile strains is usually prescribed by a set of time varying curves in existing studies [19,26] rather than using a set of ordinary differential equations by taking into account detailed tension-development mechanism as in the active stress approach [13,27]. For example, few studies have incorporated the length-dependent and force-velocity relationships into the formulation of $\mathbf{F}_a$ that have been widely studied in the active stress approach [27].

The main constituent of the myocardium is myocytes, which take about 75% of the solid volume. At the cellular level, the myocyte contains bundles of contractile myofibrils whose basic unit is sarcomere, which is about 2μm in length. The spatial arrangements of main functional elements have been reported in many studies [28–30]. In brief, sarcomere can be considered as a symmetric structure in which the actin (thin) filaments are in parallel to the myosin (the thick filament). The Z-bands at both ends are anchored to the thin filaments and linked to the myosin by the elastic protein titin. Cross-bridges can be formed between the myosin and the actin filaments, which is triggered by the action potential. In the absence of activation, the thick and thin filaments will slide relatively freely because of no formed cross-bridges, and thus the passive response of myocytes is mainly from titin, membrane, collagen and elastic fibres. Once activated, cross-bridges will be formed and strongly bind the thin and thick filaments. Through a series of "power-strokes" [31], the thin filaments will slide towards the sarcomere centre, and the generated active tension from cross-bridges will be transmitted through those components linked to the contractile units, i.e. the Z-band, the non-overlapped thin-filament, and the costamere [32,33], here we denote these components as the serial passive elements. Cook et al. [34] observed elastic deformation in the cellular level in their isometric contraction experiments even though the overall length of the myocyte/muscle did not change, which would suggest there exists elastic deformation in this serial passive element. Kojima et al. [35] measured the stiffness of a single actin filament, which is around 5×10^4 pN/μm. Given that the peak active force per myosin filament is around 530 pN [36], this will cause a stretch of 1.05 in the thin filament. Kojima et al. [35] further concluded that 50% of the sarcomere compliance is due to the extensibility of the thin filament. Thus the serial passive element, linked to the cross-bridges, is a necessary unit for effective active force generation and transmission.

Based on the geometrical arrangement of sarcomere [28–30], we propose a modified Hill model for active tension development with two branches as shown in Fig. 1, the left panel: the passive branch responsible for passive properties when no cross-bridges formed (e.g. during diastole), and the active branch which has one serial passive element and one contractile element. The serial passive element in the active branch is a lumped unit with components involved in active force transmission, including the non-overlapped thin filament, Z-band and costamere. The contractile element is the overlapped region between the thin and thick filament which allows the application of the active strain approach through the multiplicative decomposition. We then incorporate the length-dependent and force-velocity relationships in active strain, which is further calibrated with existed experimental data. To the authors' best knowledge, this is the first time to include experimentally calibrated length-dependence and force-velocity in active strain. We then validate this novel active contraction model using three typical active contraction experiments from literature. Finally, a three-dimensional finite element (FE) left ventricle (LV) model is presented with a parameter sensitivity study.

2. Methods

2.1. Hybrid active contraction model

2.1.1. The 1-dimensional Hill model for the sarcomere unit

Inspired by the widely-used Hill-type models of muscle contraction [13,21,22], a three-element rheology model is proposed here to model myocardial mechanical behaviour as depicted in Fig. 1. It consists of two branches: the upper branch for the passive response, and the lower one for the active response, and the two branches are connected in parallel. The right panel of Fig. 1 schematically illustrates the main sub-units in a typical sarcomere, including the actin filament, myosin, titin, and the Z-band [28,37]. The passive branch is responsible for the passive response of myocytes (i.e. titin, membrane) and extracellular connective tissues (collagen fibres), which can be described by a strain energy function Ψ^p. The lower branch consists of an passive element and a contractile element in serial. The contractile element is responsible for active contraction governed by the electrophysiology-mechanics coupling, and the active tension is transmitted through the passive element to additively contribute to the total myocardial stress ($\boldsymbol{\sigma}$),

$$\boldsymbol{\sigma} = \boldsymbol{\sigma}^p + \boldsymbol{\sigma}^a, \tag{1}$$

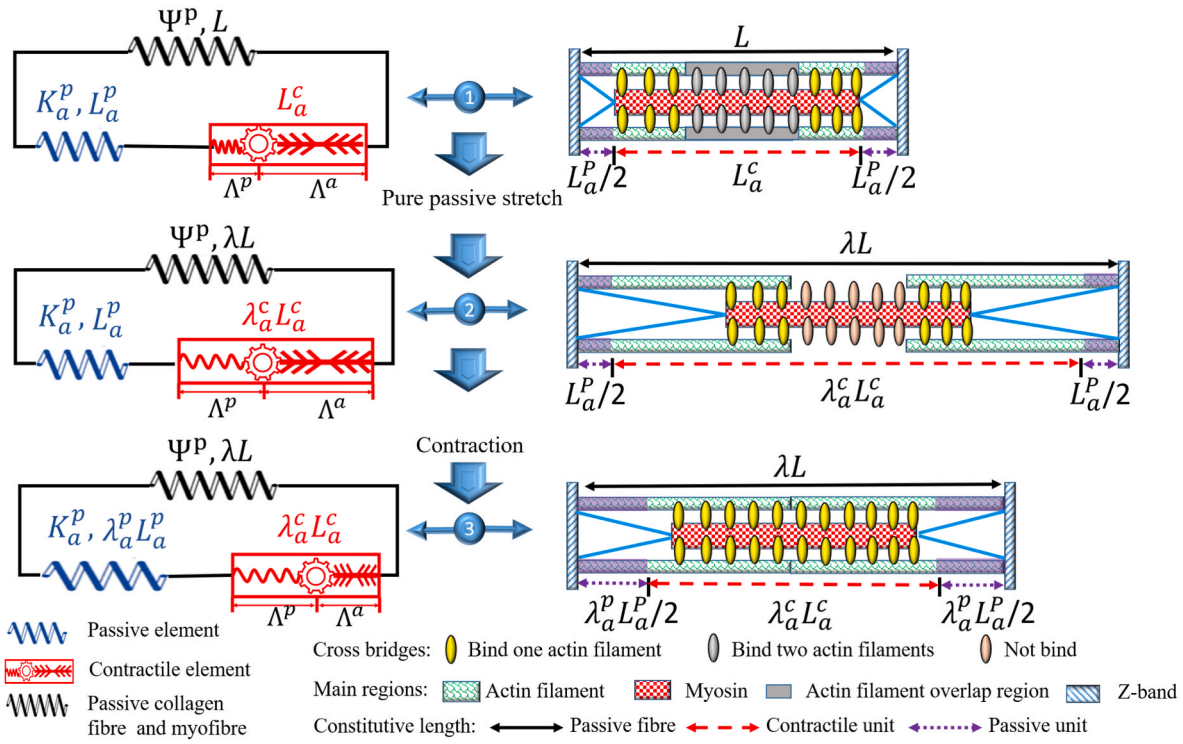

Fig. 1. A modified Hill model consisting of a parallel passive branch and an active branch (the left panel) abstracted from the microstructure of sarcomere (the right panel). This schematic illustration describes three states of a sarcomere from the resting state (top) to the passive stretching (middle), and finally the active contraction state (bottom). λ represents stretch, Λ is the stretch in the contractile element which is multiplicatively decomposed with $\lambda_a^c = \Lambda^a \Lambda^p$, L represents the length, Ψ^p is the strain energy function for the passive response, and K_a^p is the stiffness of the passive element in the active branch.

in which $\boldsymbol{\sigma}^p$ is the passive stress, and $\boldsymbol{\sigma}^a$ is the active tension which will be formulated following the active strain approach.

The geometrical features of the passive element and the contractile element are defined at stress-free state as shown in Fig. 1. We consider the overlapped region between the thick filament (myosin) and the thin filaments to be the contractile element as in [28], and further assume cross-bridges will be exclusively formed in that region. The contractile element can change its length through the sliding between the thin and thick filaments either freely (no cross-bridge formed) or active contraction. Thus, in the stress-free state, the contractile element (L_a^c) has the same length as the thick filament, 1.65μm [28]. Given that the total sarcomere length is $L = 1.85\,\mu$m at stress-free state, the passive element for transmitting active tension (L_a^p) is 0.2μm in length, i.e., $L_a^p + L_a^c = L$. See the top panel of Fig. 1 for details.

Based on the sliding filament theory, we adopt the active strain approach to model myocardial active contraction using the multiplication decomposition [21]. Thus, in this 1-D Hill model, stretch of the contractile element λ_a^c is decomposed into a fictitious inelastic/plastic component Λ^p and an active stretch Λ^a for the contractile element, that is

$$\lambda_a^c = \Lambda^a \Lambda^p, \tag{2}$$

in which the active stretch Λ^a is related to contractility and further depends on intracellular calcium transient ([Ca]), overall stretch (λ) and contraction velocity $(\dot{\lambda} = d\lambda/dt)$, and Λ^p is a fictitious stretch representing the maximum potential stretch in the contractile element under current stretch λ if no cross-bridge is formed. In other words, the multiplication of Λ^a and Λ^p mimics the sliding between the thin and thick filaments under active contraction.

2.1.2. Passive response of the active branch

In the absence of excitation, no cross-bridge will be formed between the thin and thick filaments, i.e. in diastole. We assume the contractile element can be freely stretched without any resistance since the passive response is solely from the passive branch. Then the passive element in the active branch will stay in its stress-free state because of no force generated in the active element, indicating $\lambda_a^p = 1$. Thus for the active branch without activation, we have

$$\lambda_a^p L_a^p + \lambda_a^c L_a^c = \lambda L, \tag{3}$$

where $\lambda_a^c = \Lambda^p$ is the stretch of the contractile element with $\Lambda^a = 1$ because of no active tension generation, and λ is the overall stretch of the considered sarcomere. The middle panel of Fig. 1 schematically illustrates the purely passive response process. From Eq. (3), we have

$$\Lambda^p = (\lambda L - L_a^p)/L_a^c. \tag{4}$$

2.1.3. Active response of the active branch after excitation

Once activated, a complex biochemistry process will start to form cross-bridges, causing strong bindings between the myosin heads and the thin actin filament. Through a series of "power stroke", the thick filament slides past the thin filament towards the centre of the sacromere. This phenomenon has been well described by the sliding filament theory in the literature [38]. Because of much higher active tension, in a range of 50 kPa $\sim$ 100 kPa [39], the passive element in the active branch will be stretched. The bottom panel of Fig. 1 illustrates the active contraction process. Using Eq. (3), the stretch in the passive element of the active branch is

$$\lambda_a^p = \frac{\lambda L - \lambda_a^c L_a^c}{L_a^p} = \frac{\lambda L - \lambda_a^c (L - L_a^p)}{L_a^p}. \tag{5}$$

Denoting $\eta = L/L_a^p = 9.25$, Eq. (5) can be further simplified as

$$\lambda_a^p = \lambda\eta - \lambda_a^c(\eta - 1). \tag{6}$$

Since Λ^p is the maximum fictitious passive stretch of the contractile

element under current stretch λ if no cross-bridge is formed, thus we have $\Lambda^p = (\lambda L - L_a^p)/L_a^c$, that is the same as Eq. (4) in which $\Lambda^a = 1$ without excitation. We now have

$$\lambda_a^p = \lambda\eta - \Lambda^a(\lambda\eta - 1), \tag{7}$$

and the linear strain for the passive element of the active branch is

$$\varepsilon_a^p = \lambda_a^p - 1 = (\lambda\eta - 1)(1 - \Lambda^a). \tag{8}$$

As depicted in Fig. 1, the passive element and the active element are connected in serial, thus the active tension in the active element is equal to the tension in the passive element. By assuming a linear response for the passive element, the active tension for the considered sacromerer is then

$$T^a = K_a^p \varepsilon_a^p = K_a^p (\lambda\eta - 1)(1 - \Lambda^a), \tag{9}$$

in which K_a^p is the elastic modulus of the passive element, which is set to be $K_a^p = 250$kPa. The estimation of K_a^p can be found in Appendix A. Note that the smaller Λ^a, the more shortening of the sacromerer, and the higher active tension.

2.2. Electro-mechanical coupling

Similar to [21], the evolution of Λ^a depends on the normalized intracellular calcium transient [Ca], and further governed by the action potential (AP) of myocytes. To model time varying potential of myocytes, the two-variable phenomenological Aliev-Panfilov [40] model is employed to determine [Ca] transient. The Aliev-Panfilov model includes two ordinary differential equations, one for the rapidly evolving dimensionless potential ϕ, and the other one for the slowly evolving recovery variable r. In specific,

$$\begin{aligned} \frac{\mathrm{d}\phi}{\mathrm{d}t} &= c\,\phi(\phi - \alpha)(1 - \phi) - r\,\phi, \\ \frac{\mathrm{d}r}{\mathrm{d}t} &= \widehat{\varepsilon}(\phi, r)[-r - c\,\phi(\phi - b_r - 1)], \end{aligned} \tag{10}$$

in which α, b_r and c are constants, $\widehat{\varepsilon}(\phi, r)$ is a coefficient function that governs the restitution characteristics of the AP model through additional parameters γ, μ_1 and μ_2 [21,40], and

$$\widehat{\varepsilon}(\phi, r) = \gamma + \frac{\mu_1 r}{\mu_2 + \phi}. \tag{11}$$

Similar as in [41], the normalized [Ca] transient is

$$\frac{\mathrm{d}[\mathrm{Ca}]}{\mathrm{d}t} = q\,\phi - k\,[\mathrm{Ca}] \tag{12}$$

with constant parameters k and q.

Following [41], Λ^a is defined as a function of [Ca],

$$\Lambda^a = \frac{1}{1 + \mathcal{F}([\mathrm{Ca}])(\xi - 1)}, \tag{13}$$

in which $\xi = 1/\Lambda^{\min}$, and $\Lambda^{\min}$ is the minimum stretch ratio that the active element can achieve, in other words, the maximum shortening, and the function $\mathcal{F}$ controls the contraction behaviour. The maximum value of Λ^a is 1 when there is no active contraction. Therefore, $\Lambda^{\min} \le \Lambda^a \le 1$. Similar as in Pelce et al.'s study [41],

$$\mathcal{F}([\mathrm{Ca}]) = 1 + \frac{2}{\pi}\arctan(\beta \ln\,[\mathrm{Ca}]), \tag{14}$$

where β is a constant. Note Eq. (14) is different from the study [21], a factor of two is used in this study to ensure $\mathcal{F}$ in a range of $[0, 1]$ when $[\mathrm{Ca}] \in [0, 1]$. Fig. 2 shows an example of the action potential (ϕ), the normalized intracellular calcium transient ([Ca]) and the active strain Λ^a with a fixed sarcomere length at 1.85μm under an instant stimulus of 1 that is applied at 0.1 s.

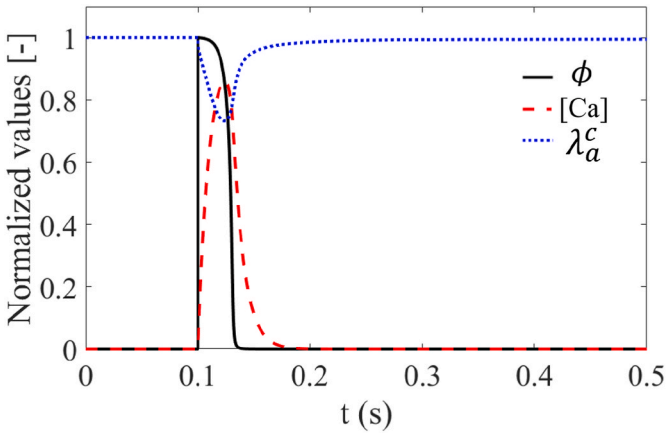

Fig. 2. The normalized action potential, the calcium concentration and the contraction of the active element using the Aliev-Panfilov model. Parameters are [21]: $\alpha = 0.01$, $\gamma = 0.002$, $b_r = 0.15$, $c = 8$, $\mu_1 = 0.2$, $\mu_2 = 0.3$, $q = 0.1$, $k = q/1$, $\beta = 3$, $\Lambda^{\min} = 0.5$ with a stimulus $\phi = 1$ at $t = 0.1$s.

Two important features of the active tension generation in myocytes are the length-dependence and force-velocity, both have been measured and studied in many cardiac muscle experiments [42,43]. The experimental study in [44] has demonstrated force-velocity curves are shifted up/down in parallel along the force axis with varied initial muscle length, suggesting the force-velocity relationship is not much affected by the muscle length, hence we assume that the force-velocity and length-dependent relationships are independent, and the minimum active stretch $\Lambda^{\min}$ is formulated as

$$\Lambda^{\min}(\lambda, \dot{\lambda}) = \begin{cases} \vartheta_1(\lambda)\vartheta_2(\dot{\lambda}) & \text{for} \quad \vartheta_1\vartheta_2 \le 1, \\ 1, & \text{otherwise}, \end{cases} \tag{15}$$

in which the function $\vartheta_1(\lambda)$ describes the length-dependent relationship, and the function $\vartheta_2(\dot{\lambda})$ is for the force-velocity relationship.

It has been widely acknowledged that there exists an optimal sarcomere length (SL) range for efficient active tension generation [45]. When outside this range, the active tension is suppressed dramatically. This indicates that $\Lambda^{\min}$ shall achieve the minimal value at this optimal SL range for maximized contraction, but with much higher values outside the optimal range. Note the smaller value of $\Lambda^{\min}$, the greater active contraction of sacromere. We now define ϑ_1 as a U-shaped quadratic function of λ, that is

$$\vartheta_1(\lambda) = \kappa_1\lambda^2 + \kappa_2\lambda + \kappa_3, \tag{16}$$

where κ_1, κ_3 are positive constants and κ_2 is a negative constant. Fig. 3(a) shows an example of ϑ_1 with varied λ, ϑ_1 reaches the minimum value (0.66) at $\lambda = 1.15$, corresponding to a stretched sarcomere at a length of 2.13μm.

For the force-velocity relationship, published experiments have demonstrated that a higher shortening velocity will reduce the active tension [13]. A zero shortening velocity corresponds to the isometric contraction with a fixed length, thus $\vartheta_2(\dot{\lambda}) = 1$ if $\dot{\lambda} = 0$. With non-zero shortening velocity, ϑ_2 will lead to a reduced active tension that can be realized by increasing $\Lambda^{\min}$. With those in mind, we choose a logistic type function for ϑ_2, specifically

$$\vartheta_2(\dot{\lambda}) = \frac{1 + \kappa_4}{1 + \kappa_4\, e^{\kappa_5\dot{\lambda}}}, \tag{17}$$

where κ_4 and κ_5 are positive parameters. It can be verified that when $\dot{\lambda} = 0$, $\vartheta_2 = 1$, and $\vartheta_2 > 1$ for any non-zero shortening velocity. Note that the shortening velocity is negative. Fig. 3(b) gives an example of ϑ_2,

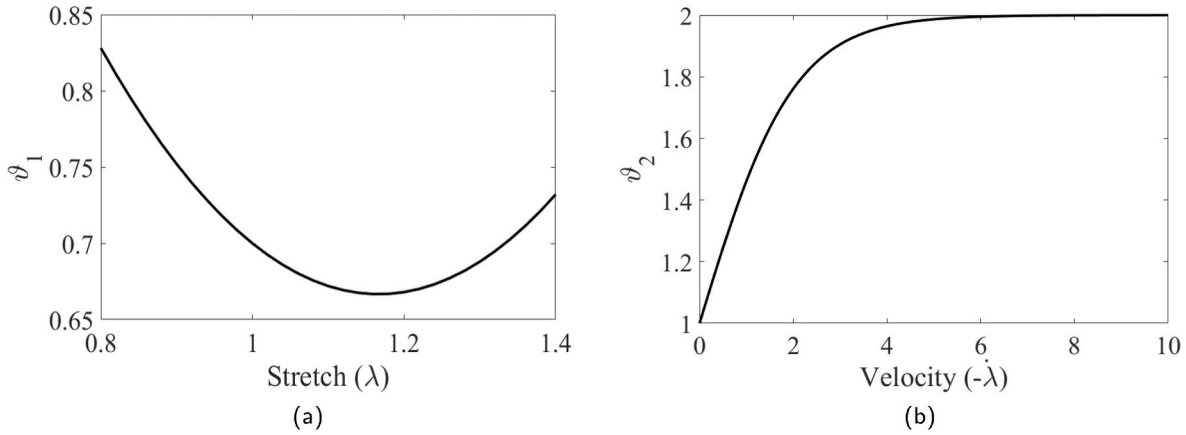

Fig. 3. Schematic illustrations of ϑ_1 and ϑ_2: (a) ϑ_1 with respect to different myofibre stretches from 0.8 to 1.4 with $\kappa_1 = 1.2$, $\kappa_2 = -2.8$ and $\kappa_3 = 2.8$; (b) ϑ_2 with respect to different myofibre contracting velocity from 0/s to −10/s with $\kappa_4 = 1.0$ and $\kappa_5 = 1.0$.

which increases with higher shortening velocity, thus weaker contraction with increased $\Lambda^{\min}$.

2.3. Upscale to 3-dimension

Assuming myocytes being analogues to homogenized sarcomeres, then the tensorial representation of the active stress in the myocyte is defined as

$$\boldsymbol{\sigma}^a = K_a^p\,(\lambda\eta - 1)(1 - \Lambda^a)\widehat{\mathbf{f}} \otimes \widehat{\mathbf{f}}, \tag{18}$$

in which $\widehat{\mathbf{f}}$ is the unit myofibre direction at the current configuration. Eq. (18) is a widely-used approach for formulating active stress in cardiac mechanics [13]. The myofibre stretch λ is

$$\lambda = \sqrt{I_{4\mathrm{f}}} = \sqrt{\mathbf{f}_0 \cdot (\mathbf{F}^{\mathrm{T}}\mathbf{F}\,\mathbf{f}_0)} \tag{19}$$

where $\mathbf{f}_0$ is the unit myofibre direction at the reference configuration, and $\mathbf{F}$ is the deformation gradient. Then Eq. (18) can be further written as

$$\boldsymbol{\sigma}^a = K_a^p(1 - \Lambda^a)\,\frac{\eta\sqrt{I_{4\mathrm{f}}} - 1}{I_{4\mathrm{f}}}\mathbf{f} \otimes \mathbf{f} \tag{20}$$

with $\mathbf{f} = \mathbf{F}\mathbf{f}_0$ and $\widehat{\mathbf{f}} = \mathbf{f}/\sqrt{I_{4\mathrm{f}}}$.

For the passive response of the myocardium, a reduced form of invariant-based strain energy function, based on the constitutive model developed by Holzapfel and Ogden [46], is used in this study with contributions from the ground matrix and myofibres,

$$\Psi^{\mathrm{p}} = \frac{a}{2b}[e^{b(I_1 - 3)} - 1] + \frac{a_{\mathrm{f}}}{2b_{\mathrm{f}}}[e^{b_{\mathrm{f}}(I_{4\mathrm{f}}^* - 1)^2} - 1], \tag{21}$$

where $a, b, a_{\mathrm{f}}, b_{\mathrm{f}}$ are material constants, $I_1 = \mathrm{trace}(\mathbf{C})$ and $I_{4\mathrm{f}} = \mathbf{f}_0 \cdot (\mathbf{C}\mathbf{f}_0)$ are strain invariants with $\mathbf{C} = \mathbf{F}^{\mathrm{T}}\mathbf{F}$. $I_{4\mathrm{f}}^* = \max(I_{4\mathrm{f}}, 1)$ is to ensure only the stretched fibres can bear load. By further assuming the myocardium is incompressible, the total Cauchy stress is then

$$\begin{aligned}\boldsymbol{\sigma} &= \boldsymbol{\sigma}^p + \boldsymbol{\sigma}^a = \mathbf{F}\frac{\partial \Psi^{\mathrm{p}}}{\partial \mathbf{F}} + \boldsymbol{\sigma}^a - p\mathbf{I} \\ &= a e^{b(I_1 - 3)}\,\mathbf{B} + 2a_{\mathrm{f}}\,(I_{4\mathrm{f}}^* - 1)\,e^{b_{\mathrm{f}}(I_{4\mathrm{f}}^* - 1)^2}\,(\mathbf{f} \otimes \mathbf{f}) + K_a^p(1 - \Lambda^a)\,\frac{\eta\sqrt{I_{4\mathrm{f}}} - 1}{I_{4\mathrm{f}}}\mathbf{f} \otimes \mathbf{f} - p\mathbf{I},\end{aligned} \tag{22}$$

where $\mathbf{B} = \mathbf{F}\mathbf{F}^T$, p is the Lagrange multiplier to enforce incompressibility ($\det \mathbf{F} = 1$), and $\mathbf{I}$ is the identity matrix.

2.4. Fitting to typical experiments

The unknowns for the hybrid active contraction model in Eq. (22) are the passive parameters: a, b, a_{f} and b_{f}, and the active parameters: κ_1, κ_2, κ_3, κ_4 and κ_5. Other active parameters including β, α, b_r, c, μ_1, μ_2, γ, k and q are obtained from the existed study [21], unless specified. In order to determine those unknown parameters, three typical experimental studies are selected: (a) the isometric contraction with different pre-stretches bathed in a saturated calcium solution [39]; (b) the constant force-velocity experiments with saturated calcium concentration [13], and (c) the isometric active tension with varied intracellular calcium transient [47]. Parameters are inferred by formulating a non-linear least-square minimization problem [48], which is implemented using the Matlab function *fmincon* (MatLab, MathWorks 2017) with the loss function

$$L(\boldsymbol{\Theta}) = \sum\nolimits_{n=1}^{N}\,[\sigma_n(\boldsymbol{\Theta}) - \sigma_n^{\exp}]^2, \tag{23}$$

where $\boldsymbol{\Theta}$ denotes the set of unknown parameters, N is the total number of data points, the scalar σ_n is the model-predicted stress component according to the corresponding experiment, and $\sigma_n^{\exp}$ is the measured value.

2.4.1. Length-dependent tension experiment

Hawkins et al. [39] measured the total, passive, and active stresses in the rat tibialis anterior muscle under different fixed stretch ratios. Passive stress was firstly measured by stretching the muscle to a fixed stretch ratio, followed by the isometric active contraction with saturated intracellular calcium transient, the total stress was then recorded. The active stress was calculated by subtracting previously measured passive stress from the total stress. To mimic Hawkins's experiment, we consider a muscle strip under uniformly unaxial stretch (λ) along muscle fibres without active contraction in the first step, then followed by the isometric active contraction with [Ca] = 1. The deformation gradient tensor is assumed to be homogeneous,

$$\mathbf{F} = \lambda\mathbf{e}_1 \otimes \mathbf{e}_1 + \frac{1}{\sqrt{\lambda}}\mathbf{e}_2 \otimes \mathbf{e}_2 + \frac{1}{\sqrt{\lambda}}\mathbf{e}_3 \otimes \mathbf{e}_3 \tag{24}$$

in which $\mathbf{e}_1$ is the unit muscle fibre direction, $\mathbf{e}_2$ and $\mathbf{e}_3$ are the cross-fibre directions. The stretch is applied along $\mathbf{e}_1$ at one end and the other end is fixed with free boundary conditions at cross-fibre directions. From Eq. (22), the passive and active tension along $\mathbf{e}_1$ are given by

$$\begin{aligned}\sigma_{11}^p &= a(\lambda^2 - \frac{1}{\lambda})e^{b(\lambda^2 + \frac{2}{\lambda} - 3)} + 2a_{\mathrm{f}}\,\lambda^2(\lambda^2 - 1)\,e^{b_{\mathrm{f}}(\lambda^2 - 1)^2}, \\ \sigma_{11}^a &= K_a^p(1 - \Lambda^a)(\lambda\eta - 1).\end{aligned} \tag{25}$$

According to the experimental protocols [39], we set $[\mathrm{Ca}] = 1$ and $\dot{\lambda} = 0$ for the isometric contraction, and

$$\sigma^a_{11} = K^p_a[1 - (\kappa_1\lambda^2 + \kappa_2\lambda + \kappa_3)](\lambda\eta - 1). \tag{26}$$

To determine those unknown parameters, we first fit σ^p_{11} to the measured passive stresses to infer the four passive parameters a, b, a_f and b_f, and then fit the active stress σ^a_{11} to the measured active stresses to determine κ_1, κ_2 and κ_3.

2.4.2. Force-velocity experiment

Land et al. [13] recently reported the constant velocity shortening experiments on human myocytes. In their experiments, the sarcomere was firstly stretched to 2.3 μm, and then the isotonic contraction was induced by releasing one end while fixing the other end. They found that the sarcomere was shortened by $7 \sim 11\%$ in a duration of $0.1 \sim 0.3$ s under a steady [Ca] concentration. In order to model Land's constant velocity shortening experiments, we assume the sarcomere is shortened by the same distance but with different duration, thus different velocities. By setting $[\mathrm{Ca}] = 1.0$, from Eq. (9), the active tension (σ^a_{pre}) before releasing is

$$\begin{aligned}\sigma^a_{\mathrm{pre}} &= K^p_a(\lambda_0\eta - 1)(1 - \Lambda^a)\\ &= K^p_a(\lambda_0\eta - 1)\left[1 - (\kappa_1\lambda_0^2 + \kappa_2\lambda_0 + \kappa_3)\right],\end{aligned} \tag{27}$$

in which the overall stretch $\lambda_0 = 2.3/1.85 \approxeq 1.24$. After releasing, the active tension (σ^a_{rel}) at end of the shortening is

$$\begin{aligned}\sigma^a_{\mathrm{rel}} &= K^p_a(\lambda_1\eta - 1)(1 - \Lambda^a)\\ &= K^p_a(\lambda_1\eta - 1)\left[1 - (\kappa_1\lambda_1^2 + \kappa_2\lambda_1 + \kappa_3)\frac{1 + \kappa_4}{1 + \kappa_4\, e^{\kappa_5\dot{\lambda}}}\right],\end{aligned} \tag{28}$$

in which $\dot{\lambda}$ represents the constant shortening velocity, and the final overall stretch $\lambda_1 = 1.12$ is about 10% reduction from λ_0 that ensures $\dot{\lambda}$ in the experimental range [0.2/s,1.2/s] [13]. The relative active tension reduction due to the shortening velocity is

$$R = \frac{\sigma^a_{\mathrm{rel}}}{\sigma^a_{\mathrm{pre}}} = \frac{(\lambda_1\eta - 1)\left[1 - (\kappa_1\lambda_1^2 + \kappa_2\lambda_1 + \kappa_3)\frac{1+\kappa_4}{1+\kappa_4\, e^{\kappa_5\dot{\lambda}}}\right]}{(\lambda_0\eta - 1)\left[1 - (\kappa_1\lambda_0^2 + \kappa_2\lambda_0 + \kappa_3)\right]}. \tag{29}$$

To fit Eq. (29) to the force-velocity experimental data, we first fix κ_1, κ_2 and κ_3 with values inferred from the length-dependent tension experiment [39], κ_4 and κ_5 are then determined by matching R to the corresponding data in Land's study [13]. In specific, we first fit a second order polynomial curve to Land's force-velocity experimental data, we then match Eq. (29) to the fitted polynomial curve by minimizing the mismatch.

2.4.3. Isometric contraction with time-evolving [Ca] concentration

Janssen & Tombe [47] measured isometric active tension with time-evolving calcium concentration by using an iterative computer feedback system, which would prevent the shortening of the central segment of rat cardiac trabeculae. Active tetanus was stimulated by maintaining a constant sarcomere stretch ($\lambda_0 = 1.189$) for the central segments. The calcium transient was increased to around 1 mM for a period of 15 min at 0.5 Hz. Because of fixed length in the central region, $\dot{\lambda} = 0$, and the active tension is then

$$\sigma^a = K^p_a\left[1 - \frac{1}{1 + \mathcal{F}([\mathrm{Ca}])(\xi - 1)}\right](\eta\lambda_0 - 1). \tag{30}$$

To model the time evolving intracellular calcium transient ([Ca]), the Aliev-Panfilov model is used here. In the fitting process, we first fit a cubic-spline curve to Janssen & Tombe's experimental data, and then match Eq. (30) to the fitted curve. A scaling parameter r_a is applied to the constants κ_1, κ_2, and κ_3 obtained from the length-dependent experiments [39], and we further optimise the parameters in the Aliev-Panfilov model to match the time course of active contraction. In sum, the optimised parameters are $\alpha, \gamma, b_r, c, \mu_1, \mu_2, q, k, \beta$ and r_a. The Aliev-Panfilo model (Eq. (10)) is solved by using the semi-explicit Matlab ODE solver *ode15s* (MatLab, MathWorks 2017).

2.5. An in vivo human heart model

A healthy human LV model from our previous study [49] is used to simulate cardiac dynamics using this new hybrid active contraction model. Fig. 4 (a) shows the in vivo image-derived LV geometry with a rule-based fibre structure where myofibres linearly rotate from the epicardium ($-60°$) to the endocardium ($60°$). A simplified circulation system [50] is attached to the LV model to provide physiological pressure and blood flow boundary conditions, including the aorta, the left atrium, the aortic valve and the mitral valve (Fig. 4 (b)). Both valves are modelled using a diode and a resistance to only allow uni-directional flow. Time-varying [Ca] transient is determined using the Aliev-Panflov model. We further assume the whole heart contracts simultaneously without time-delay due to the action potential propagation. The same assumption is widely used in modelling healthy left ventricles [12,21,49].

This LV model is implemented in ABAQUS (Dasssult Systemes, Johnston RI, USA) similar as [8,50]. The LV pressure is firstly preloaded to a population-based end-diastolic pressure (8 mmHg) [10] within 0.5 s due to lack of invasive pressure measurement. Then, the iso-volumetric contraction begins which is triggered by increased [Ca] transient, and followed by the systolic ejection when the LV pressure exceeds the aortic pressure (82 mmHg, a population-based value), finally the ejection ends when the LV pressure is lower than the aortic pressure. The next cycle starts when the LV is relaxed with a low pressure near zero. Detailed implementation of this ABAQUS-based cardiac model can be found in [51], which has been adopted in various studies [8,11].

A time-average approach is used to determine myocardial contraction velocity, that is

$$\dot{\lambda} = \frac{\lambda - \lambda^{\mathrm{ed}}}{t - t^{\mathrm{ed}}}, \tag{31}$$

in which λ is the my fibre stretch at time t, and λ^{ed} is the value at end of diastole (t^{ed}). Furthermore, to accelerate the isovolumetric relaxation after ejection so that the LV pressure can quickly return to zero, a decay function $\mathcal{H}(t)$ is applied to $\mathcal{F}([\mathrm{Ca}])$ as follows,

$$\begin{aligned}&\mathcal{F}([\mathrm{Ca}]) = \mathcal{H}(t)\,\mathcal{F}([\mathrm{Ca}]),\\ &\mathcal{H}(t) = \begin{cases}\dfrac{\exp[(t - t^{\mathrm{eject}})]}{\exp[\omega(t^{\mathrm{iso}} - t^{\mathrm{eject}})]} & \text{for} \quad t^{\mathrm{eject}} \le t \le t^{\mathrm{iso}},\\ 1, & \text{otherwise},\end{cases}\end{aligned} \tag{32}$$

where ω controls the decreasing ratio, and we set $\omega = 50$, t^{eject} is the time when the AV is closed and t^{iso} is the time when isovolumetric relaxation finishes. Since this study is not focusing on the myocardial relaxation, thus the duration of isovolumetric relaxation will have little effect on diastolic filling and active contraction. Given that, we set t^{iso} to be 0.1 s after t^{eject}. Note the isovolumetric relaxation in this study can also be treated as a pseudo-relaxation process but not in real-time or subject-specific.

2.6. Sensitivity study on active contraction parameters

A grand challenge in the development of cardiac mechanical models is to determine model parameters' identifiability, which can be approached by sensitivity analysis, including both global sensitivity analysis and local sensitivity analysis; see [52] for a review. Sensitivity analysis focuses on how parameter variations contribute to the variance of the chosen quantities of interest. Sensitivity analysis has been widely

applied to cardio-vascular modelling [53], a recent study on cardiac mechanic modelling can be found in [54]. Global sensitivity analysis usually requires running a large number of simulations, which can be very computationally demanding, recent efforts have been focused on using computationally cheap surrogate models to replace computationally expensive cardiac models, i.e., Gaussian process [55]. Instead, local sensitivity analysis merely perturbs model parameters near a set of fixed values and analyses how such small variations influence the model outputs. To shed light on the importance and identifiability (i.e., correlation) of parameters in our newly developed active contraction model, we carry out a local sensitivity study for selected active contraction parameters ($\{\theta_i, i=1,\dots,6\} := \{K_a^p, \kappa_1, \kappa_2, \kappa_3, \kappa_4, \kappa_5\}$) using the human LV model, similar to our previous study [56]. Parameters related to electrophysiology are not considered in this section. To measure the active contraction, strains along the circumferential ($\mathbf{c}_0$), radial ($\mathbf{r}_0$) and longitudinal ($\mathbf{l}_0$) directions are defined as

$$\varepsilon_c = \mathbf{c}_0 \cdot (\mathbf{E}\mathbf{c}_0), \quad \varepsilon_r = \mathbf{r}_0 \cdot (\mathbf{E}\mathbf{r}_0), \quad \varepsilon_l = \mathbf{l}_0 \cdot (\mathbf{E}\mathbf{l}_0), \tag{33}$$

where $\mathbf{E} = \frac{1}{2}(\mathbf{C} - \mathbf{I})$. Note strains are calculated with respect to the end-diastole state. Denoting the measurements (the output features) of the LV model

$$\{d_i, i=1,\dots,10\} = \{\varepsilon_j^k, \text{EF}\}, \quad k,j \in \{1,2,3\} \tag{34}$$

where ε_j^k is the average systolic strains along the circumferential ($k=1$), radial ($k=2$) and longitudinal ($k=3$) directions from three segments: the base ($j=1$), the mid-ventricle ($j=2$) and the apex ($j=3$) as shown in Fig. 4 (a), and the ejection fraction (EF) = (EDV - ESV)/EDV is evaluated using the end diastolic volume (EDV) and the end systolic volume (ESV).

To quantify the local sensitivity, the human LV model from the previous section is treated as the baseline model, then a variation of ± 10% is applied to $\{\theta\}$, one parameter at each time. A sensitivity matrix [56] is then constructed,

$$\mathbf{S} = \begin{bmatrix} \frac{\Delta d_1}{\Delta \theta_1} & \frac{\Delta d_1}{\Delta \theta_2} & \dots & \frac{\Delta d_1}{\Delta \theta_6} \\ \frac{\Delta d_2}{\Delta \theta_1} & \frac{\Delta d_2}{\Delta \theta_2} & \dots & \frac{\Delta d_2}{\Delta \theta_6} \\ \vdots & \vdots & \ddots & \vdots \\ \frac{\Delta d_{10}}{\Delta \theta_1} & \frac{\Delta d_{10}}{\Delta \theta_2} & \dots & \frac{\Delta d_{10}}{\Delta \theta_6} \end{bmatrix}, \tag{35}$$

where Δ denotes a variation in that variable. If the variations in any of the parameters produce similar responses, then these parameters may be correlated. To quantify the correlations, we further calculate the sensitivity coefficient matrix (SCM) from the normalized $\mathbf{S}$ [56],

$$\text{SCM}_{ij} = [\bar{\mathbf{S}}_i]^T [\bar{\mathbf{S}}_j] \quad \text{and} \quad i,j \in \{1,\dots,6\}, \bar{\mathbf{S}}_i = \frac{\mathbf{S}_i}{|\mathbf{S}_i|}, \mathbf{S}_i = \{\frac{\Delta d_k}{\Delta \theta_i}, k = 1,\dots,10\}. \tag{36}$$

If SCM_{ij} is close to ±1, then θ_i and θ_j are closely correlated. The existence of correlated parameters poses non-uniqueness when inversely determine them from experimental data. A possible remedy is to estimate one parameter only while leaving the correlated ones constant. In addition, the norm $|\mathbf{S}_i| = \sqrt{\sum_{k=1}^{10} \left(\frac{\Delta d_k}{\Delta \theta_i}\right)^2}$ reflects the sensitivity of the objective function to the variation of each parameter. In general, a parameter with low sensitivity is difficult to be estimated from limited experimental data.

3. Results

3.1. Fitting to experiments

Fig. 5 (a) shows the fitted and measured experimental stresses from Hawkins' study [39], and optimised parameters are listed in Table 1. It can be found that both the fitted active and passive stresses agree well with measured data. For the active stress, it can be found that the optimal stretch is around 1.2 with the maximum active tension. Beyond this range, it decreases. Corresponding $\Lambda^{\min}$ determined by Eq. (16) is shown in Fig. 5 (b). $\Lambda^{\min}$ reaches its minimum at 0.966 with a pre-stretch of around 1.2. When either the sacromere is over-stretched, i.e., > 1.3 or less-stretched, i.e., < 1, the contractility is reduced with a higher value of $\Lambda^{\min}$, in particular when the stretch is less than 1.

Fig. 6 shows the fitted constant velocity experiment results using Eq. (29) compared to the measured data in [13]. Optimal values of κ_4 and κ_5 are listed in Table 1. In general, our hybrid active contraction model follows the measured force-velocity relationship very well. For example, a fast contraction leads to a reduced active tension, almost to one fifth of the isometric tension before the release.

Fig. 7 (a) shows the time-varying active tension from this hybrid active contraction model compared with the experimental data [47] with a constant SL. Parameters of the Aliev–Pandflov model are $\alpha = 0.01$, $\gamma = 0.002$, $b_r = 0.15$, $c = 1$, $\mu_1 = 0.04$, $\mu_2 = 0.3$, $q = 0.015$, $k = 0.015$, and the corresponding action potential and [Ca] transient are shown in Fig. 7 (b). The length–dependent parameters ($\kappa_1 \sim \kappa_3$) are adjusted by a common factor $r_a = 1.007$ to have a maximum active tension of 53 kPa. Fig. 7 (c) shows the actual stretches in the contractile element and the passive element of the active branch with respect to their own reference configurations. The maximum stretch of the passive

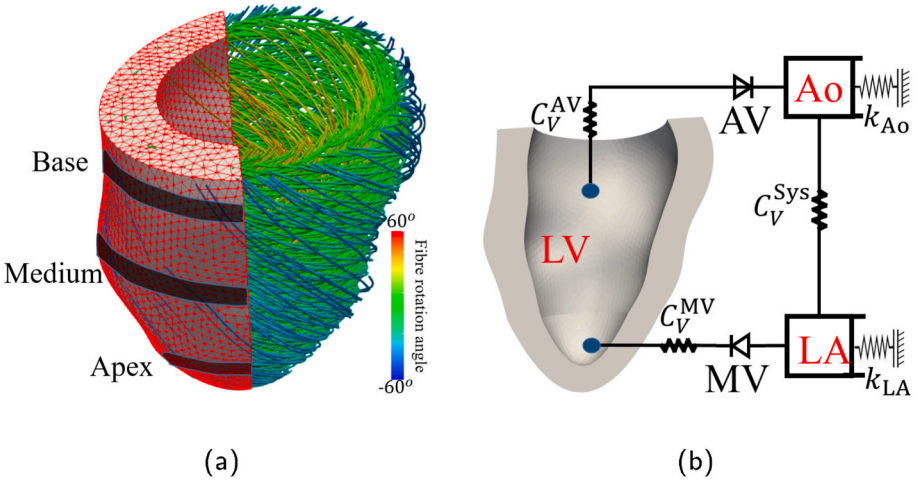

Fig. 4. (a) The human LV model (133,042 linear tetrahedral elements and 26,010 nodes) with layered myofibre structure. Three sections at the basal, middle and apical locations are defined. (b) Sketch of the human LV model with a lumped-parameter circulation model, MV: mitral valve; AV: aortic valve; LA: left atrium; Ao: aorta; Sys: systemic circulation. Grounded springs with a stiffness (k) are tuned to provide physiologically-correct pressure-volume response (i,e., compliance) in the Ao and LA cavities. C_V is the viscous resistance coefficient to describe the resistance between two cavities. Uni-directional flow through valves is controlled by setting fluid exchanging properties between the cavities. Details of the human LV model implementation can be found in [8,50].

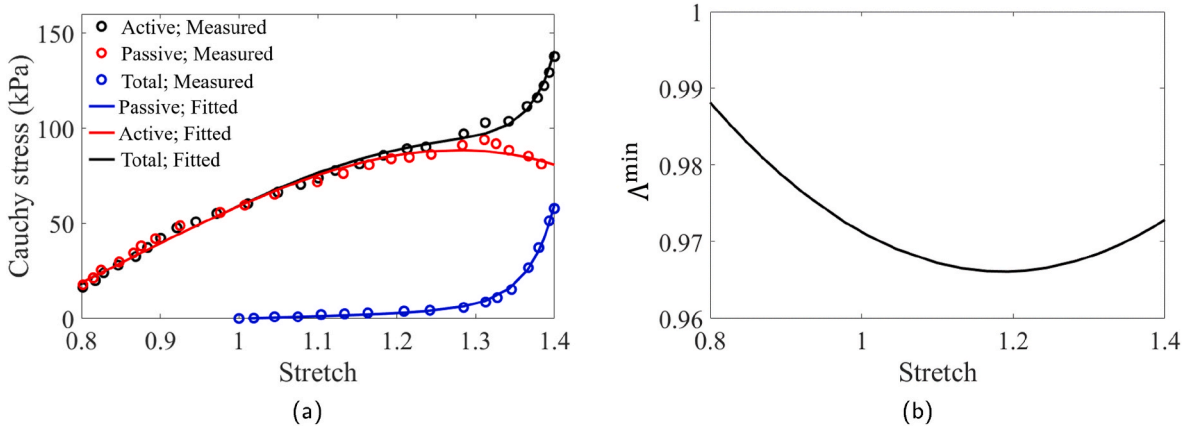

Fig. 5. Fitting the total, passive, and active stress responses in length-dependent experiments [39] (a), and the corresponding minimum active strain, i.e., $\Lambda^{\min}$, with respect to the pre-stretch of myofibre. The determined passive parameters are $a = 3.604$ kPa, $b = 0.1$, $a_f = 0.206$ kPa, and $b_f = 4.625$, other parameters can be found in Table 1.

Table 1
Optimised parameters from experimental data.

Parameters	κ_1	κ_2	κ_3	κ_4	κ_5
Hawkins et al. [39]	0.1475	−0.3500	1.1738	∼	∼
Land et al. [13]	0.1475	−0.3500	1.1738	0.0246	3.1338
Janssen and Tombe [47]	0.1485	−0.3524	1.1820	∼	∼

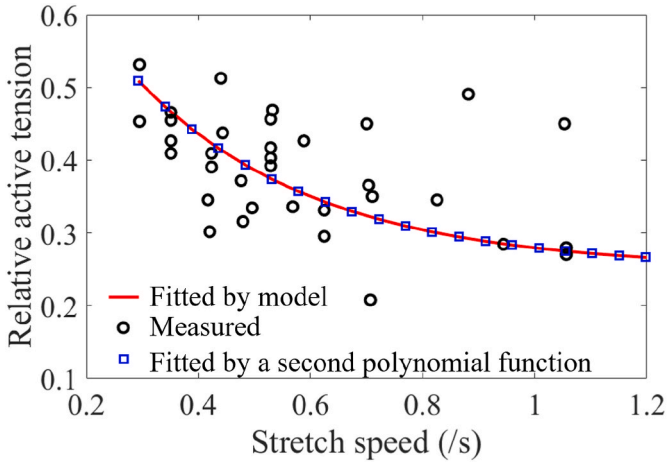

Fig. 6. Fitting results of the constant velocity shortening experiment [13].

element is around 1.21 when the active tension is the highest, and the contractile element is slightly shortened during this isometric active contraction, with a maximum shortening of 0.042μm.

3.2. The human LV model

Three cases are simulated using the human LV model, they are

- Case 1: without force-velocity in active tension by setting $\vartheta_2 = 1$, and adjusting $\kappa_1 \sim \kappa_3$ from Table 1 with a common factor r_a to achieve an EF in the physiological range of 50% ∼ 75%. Note that we do not aim to achieve a personalized simulation but to have a general healthy LV model;
- Case 2: incorporating ϑ_2 with κ_4 and κ_5 from Table 1, other parameters are the same as in case 1.
- Case 3: further adjusting r_a to achieve the same EF as in case 1.

In addition, the time-evolving [Ca] transition is determined using the experimental data from Janssen and Tombe [47] as shown in Fig. 7. Parameters for case 1 are listed in Table 2.

For case 1, we manually reduce r_a by 0.005 per step, and finally choose $r_a = 0.975$ which can lead to an EF of 57.6%. Fig. 8(a) shows the pressure-volume (p-v) loops for the three cases, which have the same end-diastolic volume because of the same end-diastolic pressures and passive properties. When including the force-velocity relation into the contraction model (case 2), the p-v loop is much smaller than that of case 1, which can be explained by the reduced active tension because of the fast contraction velocity. EF in case 2 is 26.4%, much lower than the value in case 1 (57.6%). For case 3, the re-adjusted r_a is 0.955 with nearly the same p-v loop as in case 1. The slight adjustments in length-dependent parameters may suggest that the length-dependence can play a significant role in myocyte contraction. Fig. 8(b) shows myofibre shortening ratio defined as $(\lambda - \lambda^{ed})/\lambda^{ed} \times 100\%$. The shortening ratio is much less in case 2 compared to cases 1 and 3. Again myofibre shortening ratio is almost identical in cases 1 and 3 with a peak value of

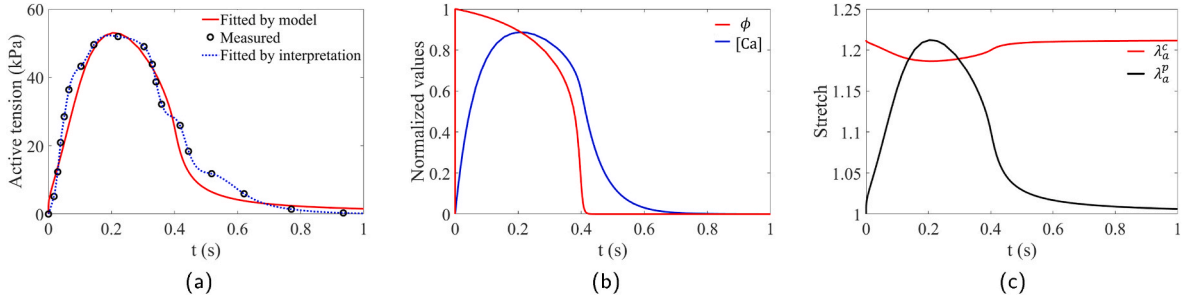

Fig. 7. Fitting results with the experimental data from [47]. (a) Active tension, (b) action potential and [Ca] transient, and (c) stretches of the contractile element and the passive element.

Table 2
Passive and active parameters in the human LV model, case 1.

Action potential	α	γ	b_r	c	μ_1	μ_2	q	k
	0.01	0.002	0.15	1.0	0.04	0.3	0.015	0.015
Active strain	K_a^p (kPa)	κ_1	κ_2	κ_3	κ_4	κ_5	β	
	250	0.1409	−0.3342	1.1210	0.0246	3.1338	3.000	
Passive response	a (kPa)	b	a_f(kPa)	b_f				
	0.22449	1.6215	2.4	1.8268				

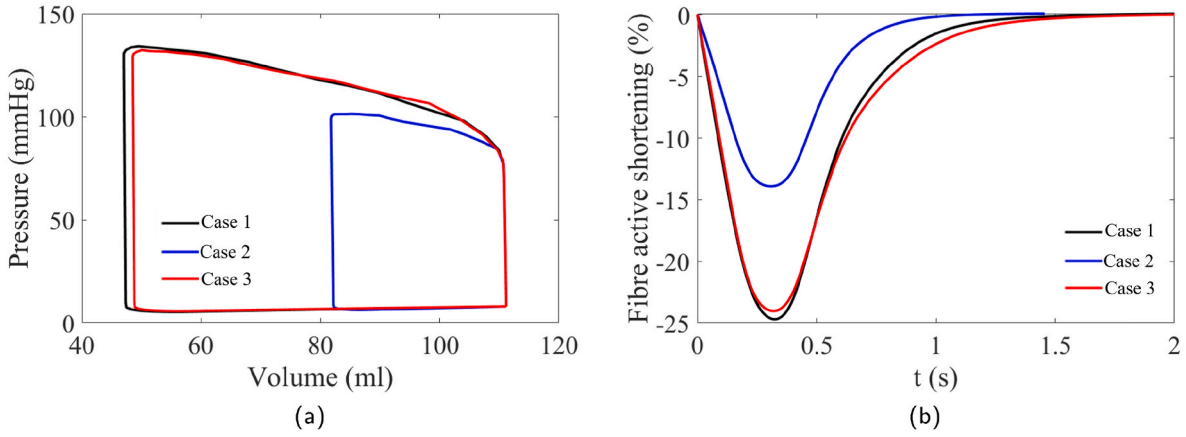

Fig. 8. Simulated LV dynamics. (a) Pressure-volume loops and (b) average myofibre shortening relative to the length at end-diastole.

−25%, which is comparable to the ratio reported from in vitro myocytes [13]. The much higher shorting ratio in the human model compared to cellular-level experiments may partially explain further parameter re-adjustment in case 3 after including the force-velocity relation, that is because the inferred parameters from cellular experiments were under different conditions compared to in vivo condition. In fact, reducing r_a is equivalent to the reduction of $\Lambda^{\min}$, in other words, increasing the contractility.

Myofibre contraction velocity ($\dot{\lambda}$) in systole is shown in Fig. 9 (a). $\dot{\lambda}$ is much more heterogeneous in case 1 at 0.1 s during systole compared to cases 2 and 3, especially near the basal region in which the myocardium contracts much faster than the middle and apical ventricle at early-systole. Because of reduced active tension in case 2, the end-systolic volume is much larger than cases 1 and 3. Corresponding myofibre stress in systole is shown in Fig. 9 (b), again much higher stress can be found for case 1 at early-systole near the base, while stress distribution patterns for the three cases are in general similar, especially at end-systole. The excessive wall thinning near the base at early-systole and thickening near the apex at end-systole in case 1 may suggest that it is necessary to include force-velocity relationship for a more homogeneous and synchronized myocardial contraction. Further experiments are needed to elucidate the exact mechanism of force-velocity relation on ventricular contraction.

3.3. Sensitivity study

Table 3 summarizes the local sensitivity analysis of the selected six parameters using case 3 as the baseline model. It can be found that κ_2 has the highest sensitivity (43.02), followed by κ_1 (42.23) and κ_4 (36.57), whilst κ_5 has the lowest sensitivity (0.06). This would suggest that both length-dependence and force-velocity play an important role in myocardial contraction. The negative correlation between K_a^p and other

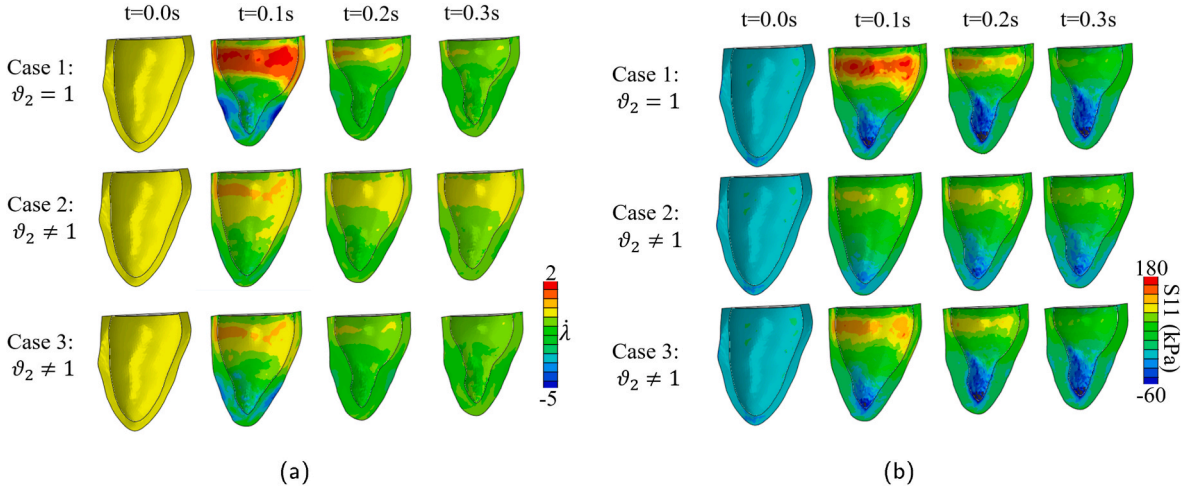

Fig. 9. Distribution of myofibre shortening at systole (a) and myofibre stress at systole(b).

Table 3
Correlation coefficient matrix and parameter sensitivities.

	K_a^p	κ_1	κ_2	κ_3	κ_4	κ_5
K_a	1.00	−0.99	−0.93	−0.84	−0.92	−0.94
κ_1		1.00	0.97	0.89	0.95	0.90
κ_2			1.00	0.98	0.98	0.77
κ_3				1.00	0.95	0.65
κ_4					1.00	0.75
κ_5						1.00
sensitivity	7.83	42.23	43.02	21.82	36.57	0.07

parameters $\kappa_1 \sim \kappa_5$ may indicate that they can compensate each other when myocardium needs to adapt its function under altered conditions. In addition, we find κ_1 and κ_2 are highly correlated (0.97). Experiments have demonstrated that when the sarcromere is prestretched to 2.2μm [45], it can achieve the maximum contraction. Since the function ϑ_1 has a maximum value at $\frac{-\kappa_2}{2\kappa_1}$, by taking $L = 1.85\mu$m and the optimal pre-stretched SL length 2.2μm, it leads to the approximation $\kappa_1 \approx -0.42\kappa_2$, the exact ratio obtained from the inferred values in Table 1.

4. Discussion

Inspired by the classic Hill's three-elements model, we have developed a hybrid active contraction model by combining active stress and active strain approaches based on the micro-structure of sarcomere, the basic contractile unit of myocytes. Different from the recent Hill's active contraction model developed by Göktepe et al. [21], we consider that the passive element in the active branch is a strictly serial element which transmits the active tension for muscle shortening, the first novelty lies. We further take into account the experimentally-calibrated length-dependence and force-velocity relationship in the active strain of the contractile element, which is missing in other active strain approaches. Our results show that this novel hybrid active contraction model can well describe existed experimental data for both the isometric contraction [39,47] and the isotonic contraction [13]. We further successfully apply this active contraction model to a beating human left ventricular model.

In this hybrid active contraction model, the passive response is described by an invariant-based phenomenal constitutive law [46,48,57,58], whilst the active response is formulated using the active strain approach based on the micro-structure of sarcomere. In sarcomere, the actin filament and myosin are the two primary units responsible for active tension generation through cross-bridges [37,59]. Analogically, the three-element Hill model usually separates the active and passive responses of sarcomere into two parallel branches: the passive and active branches as shown in Fig. 1. One element in the passive branch represents the total passive stress resulting from titin, collagen fibres, etc. The active branch has a serial structure with a passive element and a contractile element, which experiences the same tension generated from the contractile unit when it is excited. Rather than implicitly treating the serial element in the active branch to be multiplicatively attached to the contractile unit as in [21], the passive element in our model is serially attached to the contractile unit. Therefore, the active tension can also be characterized by this passive element in the active branch, for example, treating it as a linear spring as done in this study.

Length-dependent relationship is a main feature of myocyte contraction. For example, Hawkins's experiment [39] clearly showed the existence of the optimal SL at which the maximum active tension can be generated, see Fig. 5 (a). Thus, the length-dependence needs to be included in the active strain approach, as found in this study, the minimum stretch of the contractile element ($\Lambda^{\min}$) is affected by the SL length or the prestretch of sarcomere, see Fig. 5 (b). Without considering length-dependence in the active strain approach like in the classical active approach [25] or the Hill-type active contraction model developed by Göktepe et al. [21], it can be found that the active tension will keep increasing with increased pre-stretch, shown in Fig.B.1. More details can be found in Appendix B for the comparison between our model and existed active strain approaches. Therefore, there is a need to include the length-dependence in the active strain approach as being widely used in the active stress approach [13].

Contracting velocity is another factor that can affect active tension generation [13]. Rather than including contracting velocity into the cross-bridge kinematics [60] and calcium dynamics [20], we assume the contracting velocity directly affecting $\Lambda^{\min}$ based on existed experimental data. The minimum stretch of the contractile element is finally determined by the prestretch and the contracting velocity together, see Eq. (15). Our results show that the proposed force-velocity relationship for the active strain can match the experimental data well [13], and it further leads to a more homogeneous and synchronized contraction in the human LV model as shown in Fig. 9. Note, the mean contracting velocity with respect to the end-diastolic state is used for the human LV model. Our tests using the instantaneous velocity led to convergence issue and much longer computation time, which may be caused by the explicit implementation of this LV model, but not considering the viscoelasticity [60] and blood flow within the LV wall and in the cavity [61]. Nevertheless, our results from the human LV model again suggest that it is necessary to include the force-velocity relationship into active contraction.

As can be seen from Eq. (15), a non-zero contracting velocity will reduce the contractility by augmenting $\Lambda^{\min}$, which is the very reason for the poor pump function of case 2 after introducing the force-velocity relationship into active contraction. Niederer et al. [27] found that the length-dependent active tension development is key for the beat-to-beat regulation of cardiac function by using a patient-specific electro-mechanics heart model. For case 3 of the human LV model, we adjust the length-dependent parameters (κ_1, κ_2 and κ_3), which mimics the length-dependent regulation of tension development, then the LV model can achieve similar pump function as case 1. The explicit incorporation of length-dependent regulation in the active strain model would allow constructing a more biophysically accurate cardiac model.

The range of $\pm$10% around baseline values has been widely used when performing local sensitivity analysis [56,62,63]. In our human LV model, a total of $\Delta = 20\%$ of each parameter is able to produce varied model outputs. Note other ranges can also be chosen, while it is expected the results of the local sensitivity analysis will not be affected by changing the parameter ranges if such variations are still within the perturbations of baseline parameters, for example, the sensitivity ranking and correlations summarized in Table 3. While one must keep in mind the fact that such sensitivities are only local quantities and extrapolating far from the nominal value may be misleading [63]. To gain a full understanding of the model parameters in this new active contraction model, future studies shall include a global sensitivity study. From the local sensitivity study, we find two parameters κ_1 and κ_2 exhibit high correlations, indicating κ_1 could be estimated by κ_2 or vice versa, and their high correlation is reflected by the function ϑ_1 with a minimum at $-\kappa_2/(2\kappa_1)$. Since the resting sarcomere length and its optimal range vary little across different species, in fact, we can further reduce one parameter either κ_1 or κ_2 in ϑ_1. The stiffness of the passive element in the active branch K_a^p is negatively correlated to the length-dependent and force-velocity parameters, suggesting that myocytes could regulate active tension either through the passive element or the contractile unit. The poor correlation between the length-dependence and the force-velocity parameters suggests that both length-dependence and force-velocity play an essential role in active tension development.

The Aliev-Panfilov model has been widely used to study AP propagation in 2-D and 3-D cardiac tissues [64] and in realistic heart geometries [21] by providing a realistic shape of the AP with less computational demand. It can be applied to modelling both the normal

heartbeats and arrhythmias [65]. In this study, the Aliev-Panfilov model is mainly used to provide a realistic AP to trigger the active contraction but not the AP propagation, thus the choice of an AP model is not critical, which can be replaced by other models that can also provide a realistic AP shape together with the intracellular calcium transit, for example, the O'Hara-Rudy model for human myocytes [66]. Given that this study focuses on cardiac mechanics, the AP model is only used to provide the activation time, thus we did not study the existence and uniqueness of the solution for the Aliev-Panfilov model. Interested readers may refer to literature [67,68] for the analysis in those aspects.

Because of the complex LV geometry, non-linear material property and large deformation of the myocardium, cardiac mechanics model, i.e., the LV model, does not admit a closed-form solution, therefore the solution of the LV model has to be computed numerically. Various numerical approaches have been developed in the literature, among which finite element method is one of widely used numerical methods for efficiently solving nonlinear mechanics models [4]. In particular, the commercial ABAQUS software is a popular platform for developing different types of cardiac mechanics models ranging from single ventricle [69] to 4-chamber whole-heart [51], etc. In this study, the LV model is implemented and solved using ABAQUS similar to our previous studies [8,50,69] and others [11,51]. Except for finite element method, meshless methods have also been developed to solve cardiac mechanics problems [70], and partial differential equations in general [71], such as immersed boundary method with finite element extension [72], smoothed particle hydrodynamics [73], to name some. See [70] for a recent review on meshless models in cardiac mechanics.

Finally, we would like to mention limitations in this study. Firstly, we have not modelled the cross-bridge dynamics [74] in the active strain approach, thus the developed contraction model is still phenomenological, i.e., the force-velocity and length-dependence formulations, which shall be modelled with detailed biophysics in future studies as in the active stress approach [13,75]. Secondly, the active contraction is triggered by a spatially-homogeneous time-varying intracellular calcium transient, and a coupled electromechanics cardiac model would further deepen the understanding of length-dependence and force-velocity in active contraction. In addition, the selected experimental studies from Hawkins et al. [39] and Janssen & Tombe et al. [47] did not directly measure individual myocyte's contraction but inferred from muscle strips. Given the challenge and complexity of measuring active tension in single myocyte or sarcomerer, those muscle experiments still serve essential measurements to inform new model development, usually by assuming all myocytes mechanically behave the same in one experiment. In this study, we consider all myocytes in the LV contract simultaneously without time delay since the mechanical contraction takes much longer time (400 ms) than the AP propagation in a healthy LV ($\approx$ 40 ms). Therefore the AP model is simplified by using two ODE functions without spatial derivatives. However, if the AP propagation becomes significant, such as in patients with myocardial infarction, then the cardiac model shall take into account the AP propagation, which can be well described by either the bi-domain or mono-domain models [76]. Within the myocyte, its active contraction may also be described by partial differential equations [77], while such approach can be very computationally expensive for a whole heart model.

5. Conclusion

In this study, we have developed a novel hybrid active contraction model for the myocardium based on the Hill model by additionally decomposing the total stress into a passive and active response, and the active stress is further formulated following the active strain approach in the sarcomere level. Different from the multiplicative decomposition of the deformation gradient in the active strain approach, a serial passive element is considered in the active branch for transmitting the active tension, with an estimated stiffness of 250 kPa. We further incorporate the length-dependent and force-velocity relationships into the active strain response, which is depended upon the intracellular calcium concentration that is evolved with the transmembrane potential described by the Aliev-Panfilo model. The passive response is characterized by an invariant-based strain energy function that takes into account layered myofibre structures. We have demonstrated that the proposed active contraction model has a higher descriptive capability for various active contraction experiments, including both the isometric and isotonic contraction compared to existing active strain approaches. We then show that this active contraction model is applicable to the modelling of human cardiac dynamics, with more homogeneous and synchronized contraction when the active contraction model includes both the length-dependence and force-velocity relationships, whose importance is further shown from the sensitivity study by using a human LV model. Our results further show that there exists a tight interaction between the length-dependence and force-velocity relationships. The LV ejection fraction can be reduced by half from a normal range if only including the force-velocity without adjusting the length-dependence relationship. Future development can be readily expanded by including more biophysically detailed cross-bridge kinetics in this new active contraction model to reveal the fundamental mechanism of the dysregulated excitation-contraction coupling under various pathological conditions.

Acknowledgments

We are grateful for the funding provided by the UK EPSRC (EP/N014642/1, EP/S030875, EP/S020950/1, EP/S014284/1, EP/R511705/1) and H.G. further acknowledges the EPSRC ECR Capital Award (308011). L.C. acknowledges the National Science Foundation of China (11871399). D.G. also acknowledges funding from the Chinese Scholarship Council and the fee waiver from the University of Glasgow.

Data availability

The datasets supporting this article have been uploaded to Github as part of the electronic supplementary material, https://github.com/HaoGao/HybridActiveContraction.

Appendix A. Estimating K_a^p

Experimental data on active tension are mostly done in the tissue level [39,42,47] or in the cellular level [13]. In order to estimate K_a^p, we assume myocyte having the same analogous structure as the sarcomere shown in Fig. 1, the left panel. We then lump the thin-filament in the I-band, Z-bands and costamere together to the passive element in the active branch with a resting length of 0.2 μm, and considering they all are responsible for active tension transmission. Thus, the active tension of a myocyte is

$$K_a^p \varepsilon_a^e = \frac{Nf}{A_0}, \tag{A.1}$$

where ε_a^e is the strain of the passive element, N is the total number of sarcomeres in one myocyte, f is the active force per sarcomere, and A_0 is the cross-

section area of the myocyte. The stiffness of costamere is around 30pN/μm, much softer than the actin filament which has a stiffness of around 5×10^4 pN/μm [35]. We further assume that the stiffness of the passive element in the active branch will be mainly determined by the stiffness of costamere. Moreover, the analogous structure assumption indicates the myocyte and the sarcomere will share the same strain (ε_a^e). Then the active force for each sarcomere could be approximated as

$$f = K_s\, \varepsilon_a^e\, L_a^p, \tag{A.2}$$

in which K_s is the stiffness of the passive element in the active branch, taken to be the stiffness of costamere. Note the unit for K_s is pN/μm but not Pa, thus the length of the passive element L_a^p is included in Eq. (A.2). Substituting Eq. (A.2) into Eq. (A.1), we have

$$K_a^p = \frac{N\, K_s\, L_a^p}{A_0}. \tag{A.3}$$

The spatial lattice of sarcomere is an equal hexagon with a side length about 27 nm [78], and its cross-sectional area is around $a_0 = 1.728 \times 10^{-15}\,\mathrm{m}^2$. There are about 72.2 sarcomeres longitudinally along one myocyte in average [79], then the total number of sarcomere in one myocyte is $N = 72.2A_0/a_0$. From Eq. (A.3), we have $K_a^p = 250$kPa, which is also in a similar range of the active tension (270 kPa) as reported in [36]. We also have tried different values of $K_a^p \in [100{,}500]$kPa when fitting the active contraction model to the experimental data from [39], excellent agreement has been achieved with $K_a^p > 100$kPa, this further suggests that the selected $K_a^p = 250$kPa is reasonable. It is worthy to mention that this is a simplified estimation of K_a^p, and may be only considered to a homogenized stiffness of the passive element in the active branch, but not the stiffness of a specific sub-unit. Future development of this active contraction model shall include individual sub-units in active force transmission to avoid the lumped stiffness estimation.

Appendix B. Comparing with existed active strain approaches

In this section, we further compare two existed active contraction models by fitting them to the length-dependent experimental data from Hawkins et al. [39], they are the classical active strain model [14,25] and a Hill's three–element model developed by Göktepe et al. [21]. Both models are based on the multiplicative decomposition of the total deformation gradient ($\mathbf{F}$) [15] as

$$\mathbf{F} = \mathbf{F}_\mathrm{E}\mathbf{F}_\mathrm{A}, \tag{B.1}$$

where $\mathbf{F}_\mathrm{A}$ is the inelastic active deformation tensor and $\mathbf{F}_\mathrm{E} = \mathbf{F}\mathbf{F}_\mathrm{A}^{-1}$ is the elastic deformation tensor.

In the classical active strain model [14,25], the total myocardial stress is derived from a chosen strain energy function with $\mathbf{F}_\mathrm{E}$, and the active stress is not explicitly defined. For example, by assuming contraction only occurs along the myofibre direction, the active deformation tensor can be defined as

$$\mathbf{F}_\mathrm{A} = \mathbf{I} + (\lambda_a - 1)\mathbf{f}_0 \otimes \mathbf{f}_0, \tag{B.2}$$

and its inverse is $\mathbf{F}_\mathrm{A}^{-1} = \mathbf{I} + (\frac{1}{\lambda_a} - 1)\mathbf{f}_0 \otimes \mathbf{f}_0$. Here λ_a describes the contraction of myofibres, which further depends on time [19] and [Ca] [21,80]. In this study, λ_a is similar to Eq. (14), that is

$$\lambda_a([\mathrm{Ca}]) = \frac{1}{1 + \mathcal{F}([\mathrm{Ca}])(\frac{1}{\lambda_{\min}} - 1)}, \tag{B.3}$$

where $\lambda_{\min}$ is a constant which will be determined from the experimental data, and it is different from $\Lambda^{\min}$. The elastic deformation tensor is then

$$\mathbf{F}_E = \mathbf{F} + (\frac{1}{\lambda_a} - 1)\mathbf{F}\,\mathbf{f}_0 \otimes \mathbf{f}_0. \tag{B.4}$$

From Eq. (21), the total Cauchy stress is

$$\boldsymbol{\sigma} = J_E^{-1}\mathbf{F}_E\frac{\partial \Psi^\mathrm{p}}{\partial \mathbf{F}_E} = J_E^{-1}\, a\, e^{b(I_1^E - 3)}\, \mathbf{B}_E + 2J_E^{-1}\, a_\mathrm{f}\, (I_{4\mathrm{f}}^{E*} - 1)\, e^{b_\mathrm{f}(I_{4\mathrm{f}}^{E*} - 1)^2}\, (\mathbf{f}_E \otimes \mathbf{f}_E), \tag{B.5}$$

where $J_E = \det(\mathbf{F}_E)$, $\mathbf{B}_E = \mathbf{F}_E\mathbf{F}_E^\mathrm{T}$, $\mathbf{f}_E = \mathbf{F}_E\mathbf{f}_0$, $\mathbf{C}_E = \mathbf{F}_E^\mathrm{T}\mathbf{F}_E$, $I_1^E = \mathrm{trace}(\mathbf{C}_E)$, $I_{4\mathrm{f}}^E = \mathbf{f}_0 \cdot (\mathbf{C}_E\mathbf{f}_0)$, and $I_{4\mathrm{f}}^{E*} = \max(I_{4\mathrm{f}}^E, 1)$. Note $\boldsymbol{\sigma}$ in Eq. (B.5) consists of both the passive and active stresses, and a non-zero active stress can not be separated from the total stress.

In the Hill's three-element approach [21], an active strain energy function (Ψ^a) is assumed with $\mathbf{F}_E$, and a passive strain energy function using $\mathbf{F}$ for purely passive response. The active stress is added up to the passive stress for the total stress. Here, we use the same active strain energy function from [21],

$$\Psi^a = \frac{\zeta}{2}(I_{4\mathrm{f}}^E - 1)^2, \tag{B.6}$$

in which ζ is an active parameter. Using the same strain energy function for the passive response (Ψ^p) from Eq. (21), the total Cauchy stress is

$$\boldsymbol{\sigma} = \boldsymbol{\sigma}^p + \boldsymbol{\sigma}^a = J^{-1}\mathbf{F}\frac{\partial \Psi^\mathrm{p}}{\partial \mathbf{F}} + J_E^{-1}\mathbf{F}_E\frac{\partial \Psi^\mathrm{a}}{\partial \mathbf{F}_E} = J^{-1}\, a\, e^{b(I_1 - 3)}\, \mathbf{B} + 2J^{-1}\, a_\mathrm{f}\, (I_{4\mathrm{f}}^* - 1)\, e^{b_\mathrm{f}(I_{4\mathrm{f}}^* - 1)^2}\, (\mathbf{f} \otimes \mathbf{f}) + 2J_E^{-1}\zeta(I_{4\mathrm{f}}^E - 1)\mathbf{f}_E \otimes \mathbf{f}_E. \tag{B.7}$$

Note for this Hill's three-element model, the active and passive stress can be fitted separately to corresponding experimental data as seen from Eq.

(B.7).

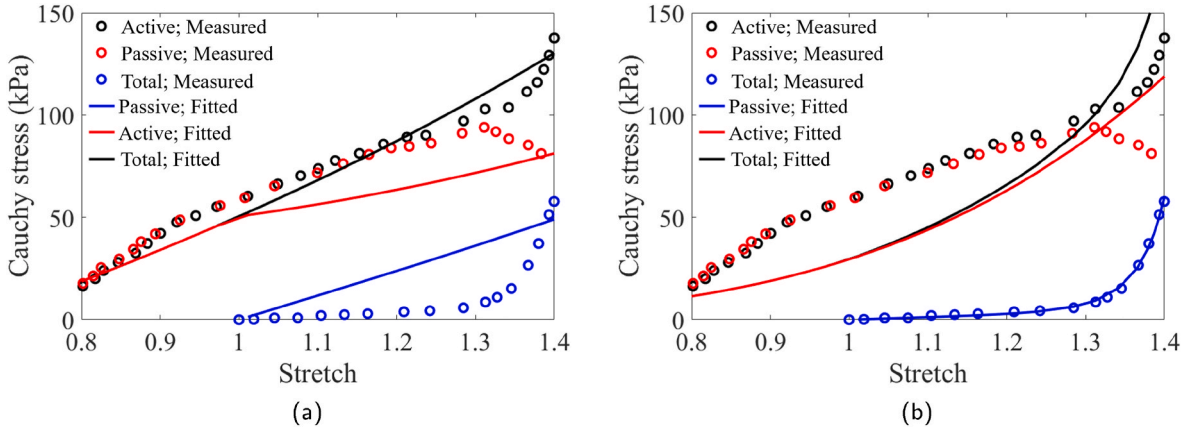

Fig. B.1. Fitting the classic active strain approach (a) and the Hill's three elements approach (b) to the length-dependent experiment [39].

Fig. B1 shows the fitted results using the classic active strain and the Hill's three-elements approaches to the experimental data from Hawkins et al. [39]. It can be seen that both active contraction models can not match the measurements. The passive response from the classic active strain model is almost linear in Fig. B1 (a), very different from the measured passive response. Similar result for the active stress, it increases monotonically with increased pre-stretch without showing an optimal stretch range, which is not physiologically accurate. For the Hill's three-elements model [21], it can fit the measured passive stress very well (Fig. B1 (b)) because of the separated passive strain energy function, and the inferred passive parameters are $a = 3.604$ kPa, $b = 0.1$, $a_f = 0.206$ kPa, and $b_f = 4.625$. However, the fitted active stress increases monotonically with increased stretch with $\zeta = 2.24$ and $\lambda_{\min} = 0.5$, which is similar as the classic active strain approach. The poor fitting result for this two approaches is largely because of a lack of length-dependence, which leads to always increased active tension with increased pre-stretch.

References

[1] Jorge Corral-Acero, Francesca Margara, Maciej Marciniak, Cristobal Rodero, Filip Loncaric, Yingjing Feng, Andrew Gilbert, Joao F. Fernandes, Hassaan A. Bukhari, Wajdan Ali, et al., The 'digital twin'to enable the vision of precision cardiology, Eur. Heart J. 41 (48) (2020) 4556–4564.

[2] Radomir Chabiniok, Vicky Y. Wang, Myrianthi Hadjicharalambous, Liya Asner, Jack Lee, Maxime Sermesant, Ellen Kuhl, Alistair A. Young, Philippe Moireau, Martyn P. Nash, Dominique Chapelle, David A. Nordsletten, Multiphysics and multiscale modelling, data–model fusion and integration of organ physiology in the clinic: ventricular cardiac mechanics, Interface Focus 6 (2) (April 2016), 20150083.

[3] Kenneth Mangion, Hao Gao, Dirk Husmeier, Xiaoyu Luo, Colin Berry, Advances in computational modelling for personalised medicine after myocardial infarction, Heart 104 (7) (April 2018) 550–557.

[4] Alfio Quarteroni, Toni Lassila, Simone Rossi, Ricardo Ruiz-Baier, Integrated heart—coupling multiscale and multiphysics models for the simulation of the cardiac function, Comput. Methods Appl. Mech. Eng. 314 (2017) 345–407.

[5] Donald M. Bers, Cardiac excitation–contraction coupling, Nature 415 (6868) (2002) 198–205.

[6] Steven A. Niederer, Kenneth S. Campbell, Stuart G. Campbell, A short history of the development of mathematical models of cardiac mechanics, J. Mol. Cell. Cardiol. 127 (2019) 11–19.

[7] Thomas SE. Eriksson, Anton J. Prassl, Gernot Plank, Gerhard A. Holzapfel, Modeling the dispersion in electromechanically coupled myocardium, Int. J. Num. Methods Biomed. Eng. 29 (11) (2013) 1267–1284.

[8] Debao Guan, Zhuan Xin, William Holmes, Xiaoyu Luo, Hao Gao, Modelling of fibre dispersion and its effects on cardiac mechanics from diastole to systole, J. Eng. Math. 128 (1) (2021) 1–24.

[9] Julius M. Guccione, L.K. Waldman, Andrew D. McCulloch, Mechanics of active contraction in cardiac muscle: Part ii—cylindrical models of the systolic left ventricle, J. Biomech. Eng. 115 (1) (1993) 82–90.

[10] Hao Gao, Andrej Aderhold, Kenneth Mangion, Xiaoyu Luo, Dirk Husmeier, Colin Berry, Changes and classification in myocardial contractile function in the left ventricle following acute myocardial infarction, J. R. Soc. Interface 14 (132) (2017), 20170203.

[11] Kevin L. Sack, Eric Aliotta, Daniel B. Ennis, Jenny S. Choy, Ghassan S. Kassab, Julius M. Guccione, Thomas Franz, Construction and validation of subject-specific biventricular finite-element models of healthy and failing swine hearts from high-resolution dt-mri, Front. Physiol. 9 (2018) 539.

[12] Martin Genet, Lik Chuan Lee, Rebecca Nguyen, Henrik Haraldsson, Gabriel Acevedo-Bolton, Zhihong Zhang, Ge Liang, Karen Ordovas, Sebastian Kozerke, Julius M. Guccione, Distribution of normal human left ventricular myofiber stress at end diastole and end systole: a target for in silico design of heart failure treatments, J. Appl. Physiol. 117 (2) (2014) 142–152.

[13] Sander Land, So-Jin Park-Holohan, Nicolas P. Smith, Cristobal G Dos Remedios, Jonathan C. Kentish, Steven A. Niederer, A model of cardiac contraction based on novel measurements of tension development in human cardiomyocytes, J. Mol. Cell. Cardiol. 106 (2017) 68–83.

[14] D. Ambrosi, S. Pezzuto, Active stress vs. active strain in mechanobiology: constitutive issues, J. Elasticity 107 (2) (2012) 199–212.

[15] V.I. Kondaurov, L.V. Nikitin, Finite strains of viscoelastic muscle tissue, J. Appl. Math. Mech. 51 (3) (1987) 346–353.

[16] Larry A. Taber, Renato Perucchio, Modeling heart development, J. Elasticity Phys. Sci. Solid. 61 (1–3) (2000) 165–197.

[17] C. Cherubini, S. Filippi, P. Nardinocchi, L. Teresi, An electromechanical model of cardiac tissue: constitutive issues and electrophysiological effects, Prog. Biophys. Mol. Biol. 97 (2–3) (2008) 562–573.

[18] Davide Ambrosi, Gianni Arioli, Fabio Nobile, Alfio Quarteroni, Electromechanical coupling in cardiac dynamics: the active strain approach, SIAM J. Appl. Math. 71 (2) (2011) 605–621.

[19] Luca Barbarotta, Simone Rossi, Dedè Luca, Alfio Quarteroni, A transmurally heterogeneous orthotropic activation model for ventricular contraction and its numerical validation, Int. J. Num. Methods Biomed. Eng. 34 (12) (2018), e3137.

[20] Ricardo Ruiz-Baier, Alessio Gizzi, Simone Rossi, Christian Cherubini, Aymen Laadhari, Simonetta Filippi, Alfio Quarteroni, Mathematical modelling of active contraction in isolated cardiomyocytes, Math. Med. Biol.: J. IMA 31 (3) (2014) 259–283.

[21] Serdar Göktepe, Andreas Menzel, Ellen Kuhl, The generalized hill model: a kinematic approach towards active muscle contraction, J. Mech. Phys. Solid. 72 (2014) 20–39.

[22] Archibald Vivian Hill, The heat of shortening and the dynamic constants of muscle, Proc. R. Soc. Lond. Ser. B Biol. Sci. 126 (843) (1938) 136–195.

[23] Ross H. Miller, B. Müller, S.I. Wolf, Hill-based Muscle Modeling. *Handbook of Human Motion*, Springer, Berlin, 2018, pp. 373–394.

[24] Sjur Gjerald, Johan Hake, Simone Pezzuto, Joakim Sundnes, Samuel T. Wall, Patient–specific parameter estimation for a transversely isotropic active strain model of left ventricular mechanics, in: International Workshop on Statistical Atlases and Computational Models of the Heart, Springer, 2014, pp. 93–104.

[25] Simone Rossi, Toni Lassila, Ricardo Ruiz-Baier, Adélia Sequeira, Alfio Quarteroni, Thermodynamically consistent orthotropic activation model capturing ventricular

systolic wall thickening in cardiac electromechanics, Eur. J. Mech. Solid. 48 (2014) 129–142.
[26] Giulia Giantesio, Alessandro Musesti, Davide Riccobelli, A comparison between active strain and active stress in transversely isotropic hyperelastic materials, J. Elasticity 137 (1) (2019) 63–82.
[27] Steven A. Niederer, Gernot Plank, Phani Chinchapatnam, Matthew Ginks, Pablo Lamata, Kawal S. Rhode, Christopher A. Rinaldi, Reza Razavi, Nicolas P. Smith, Length-dependent tension in the failing heart and the efficacy of cardiac resynchronization therapy, Cardiovasc. Res. 89 (2) (2011) 336–343.
[28] Takumi Washio, Jun-ichi Okada, Seiryo Sugiura, Toshiaki Hisada, Approximation for cooperative interactions of a spatially-detailed cardiac sarcomere model, Cell. Mol. Bioeng. 5 (1) (2012) 113–126.
[29] Francesco Regazzoni, Dedè Luca, Alfio Quarteroni, Biophysically detailed mathematical models of multiscale cardiac active mechanics, PLoS Comput. Biol. 16 (10) (2020), e1008294.
[30] Francesco Regazzoni, Dedè Luca, Alfio Quarteroni, Active contraction of cardiac cells: a reduced model for sarcomere dynamics with cooperative interactions, Biomech. Model. Mechanobiol. 17 (6) (2018) 1663–1686.
[31] Ronald D. Vale, Ronald A. Milligan, The way things move: looking under the hood of molecular motor proteins, Science 288 (5463) (2000) 88–95.
[32] Charles S. Chung, Henk L. Granzier, Contribution of titin and extracellular matrix to passive pressure and measurement of sarcomere length in the mouse left ventricle, J. Mol. Cell. Cardiol. 50 (4) (2011) 731–739.
[33] Brian Sit, Daniel Gutmann, Thomas Iskratsch, Costameres, dense plaques and podosomes: the cell matrix adhesions in cardiovascular mechanosensing, J. Muscle Res. Cell Motil. 40 (2) (2019) 197–209.
[34] C.S. Cook, M.J. McDonagh, Force responses to constant-velocity shortening of electrically stimulated human muscle-tendon complex, J. Appl. Physiol. 81 (1) (1996) 384–392.
[35] Hiroaki Kojima, Akihiko Ishijima, Toshio Yanagida, Direct measurement of stiffness of single actin filaments with and without tropomyosin by in vitro nanomanipulation, Proc. Natl. Acad. Sci. Unit. States Am. 91 (26) (1994) 12962–12966.
[36] Srboljub M. Mijailovich, Oliver Kayser-Herold, Boban Stojanovic, Djordje Nedic, Thomas C. Irving, Michael A. Geeves, Three-dimensional stochastic model of actin–myosin binding in the sarcomere lattice, J. Gen. Physiol. 148 (6) (2016) 459–488.
[37] Wolfgang A. Linke, Titin gene and protein functions in passive and active muscle, Annu. Rev. Physiol. 80 (2018) 389–411.
[38] Hugh E. Huxley, Fifty years of muscle and the sliding filament hypothesis, Eur. J. Biochem. 271 (8) (2004) 1403–1415.
[39] D. Hawkins, M. Bey, A Comprehensive Approach for Studying Muscle-Tendon Mechanics, 1994.
[40] Rubin R. Aliev, Alexander V. Panfilov, A simple two-variable model of cardiac excitation, Chaos, Solit. Fractals 7 (3) (1996) 293–301.
[41] Pierre Pelce, Jiong Sun, Cor Langeveld, A simple model for excitation-contraction coupling in the heart, Chaos, Solit. Fractals 5 (3–4) (1995) 383–391.
[42] Julius M. Guccione, Andrew D. McCulloch, Mechanics of Active Contraction in Cardiac Muscle: Part I—Constitutive Relations for Fiber Stress that Describe Deactivation, 1993.
[43] Marcel Daniels, M.I. Noble, He Ter Keurs, Bjorn Wohlfart, Velocity of sarcomere shortening in rat cardiac muscle: relationship to force, sarcomere length, calcium and time, J. Physiol. 355 (1) (1984) 367–381.
[44] Allen R. Gordon, J Siegman Marion, Mechanical properties of smooth muscle. i. length-tension and force-velocity relations, Am. J. Physiol. Legacy Content 221 (5) (1971) 1243–1249.
[45] Thomas J. Burkholder, Richard L. Lieber, Sarcomere length operating range of vertebrate muscles during movement, J. Exp. Biol. 204 (9) (2001) 1529–1536.
[46] Gerhard A. Holzapfel, Ray W. Ogden, Constitutive modelling of passive myocardium: a structurally based framework for material characterization, Phil. Trans. Roy. Soc. Lond.: Math. Phys. Eng. Sci. 367 (1902) (2009) 3445–3475.
[47] P.M. Janssen, Pieter P. de Tombe, Uncontrolled sarcomere shortening increases intracellular ca2+ transient in rat cardiac trabeculae, Am. J. Physiol. Heart Circ. Physiol. 272 (4) (1997) H1892–H1897.
[48] Debao Guan, Faizan Ahmad, Peter Theobald, Shwe Soe, Xiaoyu Luo, Hao Gao, On the aic-based model reduction for the general holzapfel–ogden myocardial constitutive law, Biomech. Model. Mechanobiol. 18 (4) (2019) 1213–1232.
[49] Hao Gao, David Carrick, Colin Berry, Boyce E. Griffith, Xiaoyu Luo, Dynamic finite-strain modelling of the human left ventricle in health and disease using an immersed boundary-finite element method, IMA J. Appl. Math. 79 (5) (October 2014) 978–1010. Conference Name: IMA Journal of Applied Mathematics.
[50] Debao Guan, Yao Jiang, Xiaoyu Luo, Hao Gao, Effect of myofibre architecture on ventricular pump function by using a neonatal porcine heart model: from dt-mri to rule-based methods, R. Soc. Open Sci. 7 (4) (2020), 191655.
[51] Brian Baillargeon, Nuno Rebelo, David D. Fox, Robert L. Taylor, Ellen Kuhl, The living heart project: a robust and integrative simulator for human heart function, Eur. J. Mech. Solid. 48 (2014) 38–47.
[52] Jerome Morio, Global and local sensitivity analysis methods for a physical system, Eur. J. Phys. 32 (6) (2011) 1577.
[53] Gary R. Mirams, Pras Pathmanathan, Richard A. Gray, Peter Challenor, Richard H. Clayton, Uncertainty and variability in computational and mathematical models of cardiac physiology, J. Physiol. (2016) 6833–6847.
[54] Alan Lazarus, David Dalton, Dirk Husmeier, Hao Gao, Sensitivity Analysis and Inverse Uncertainty Quantification for the Left Ventricular Passive Mechanics, 2022 in revision.
[55] Umberto Noè, Alan Lazarus, Hao Gao, Vinny Davies, Benn Macdonald, Kenneth Mangion, Colin Berry, Xiaoyu Luo, Dirk Husmeier, Gaussian process emulation to accelerate parameter estimation in a mechanical model of the left ventricle: a critical step towards clinical end-user relevance, J. R. Soc. Interface 16 (156) (2019), 20190114.
[56] H. Gao, W.G. Li, L. Cai, C. Berry, X.Y. Luo, Parameter estimation in a holzapfel–ogden law for healthy myocardium, J. Eng. Math. 95 (1) (2015) 231–248.
[57] Zhuan Xin, Xiaoyu Luo, Hao Gao, Ray W. Ogden, Coupled agent-based and hyperelastic modelling of the left ventricle post-myocardial infarction, Int. J. Num. Methods Biomed. Eng. 35 (1) (2019), e3155.
[58] Kewei Li, Ray W. Ogden, Gerhard A. Holzapfel, A discrete fibre dispersion method for excluding fibres under compression in the modelling of fibrous tissues, J. R. Soc. Interface 15 (138) (2018), 20170766.
[59] Melanie K. Miller, Henk Granzier, Elisabeth Ehler, Carol C. Gregorio, The sensitive giant: the role of titin-based stretch sensing complexes in the heart, Trends Cell Biol. 14 (3) (2004) 119–126.
[60] A.V.S. Ponnaluri, Le Perotti, D.B. Ennis, W.S. Klug, A viscoactive constitutive modeling framework with variational updates for the myocardium, Comput. Methods Appl. Mech. Eng. 314 (2017) 85–101.
[61] Scott I Heath Richardson, Hao Gao, Jennifer Cox, Rob Janiczek, Boyce E. Griffith, Colin Berry, Xiaoyu Luo, A poroelastic immersed finite element framework for modelling cardiac perfusion and fluid–structure interaction, Int. J. Num. Methods Biomed. Eng. (2021) page e3446.
[62] Jack F. Fowler, Sensitivity analysis of parameters in linear-quadratic radiobiologic modeling, Int. J. Radiat. Oncol. Biol. Phys. 73 (5) (2009) 1532–1537.
[63] Ryan G. McClarren, Penrose McClarren, Penrose, Uncertainty Quantification and Predictive Computational Science, Springer, 2018.
[64] Martyn P. Nash, Alexander V. Panfilov, Electromechanical model of excitable tissue to study reentrant cardiac arrhythmias, Prog. Biophys. Mol. Biol. 85 (2–3) (2004) 501–522.
[65] Sergei Pravdin, Hans Dierckx, Vladimir S. Markhasin, Alexander V. Panfilov, Drift of scroll wave filaments in an anisotropic model of the left ventricle of the human heart, BioMed Res. Int. (2015), 2015.
[66] Thomas O'Hara, László Virág, András Varró, Yoram Rudy, Simulation of the undiseased human cardiac ventricular action potential: model formulation and experimental validation, PLoS Comput. Biol. 7 (5) (2011), e1002061.
[67] Zemlyanukhin Ai, A.V. Bochkarev, Analytical properties and exact solution of the aliev-panfilov model, in: Journal of Physics: Conference Series, vol. 1205, IOP Publishing, 2019, 012060.
[68] Yves Bourgault, Yves Coudiere, Charles Pierre, Existence and uniqueness of the solution for the bidomain model used in cardiac electrophysiology, Nonlinear Anal. R. World Appl. 10 (1) (2009) 458–482.
[69] H.M. Wang, H. Gao, X.Y. Luo, C. Berry, B.E. Griffith, R.W. Ogden, T.J. Wang, Structure-based finite strain modelling of the human left ventricle in diastole, Int. J. Num. Methods Biomed. Eng. 29 (1) (2013) 83–103.
[70] Èric Lluch, Mathieu De Craene, Bart Bijnens, Maxime Sermesant, Jérôme Noailly, Oscar Camara, Hernán G. Morales, Breaking the state of the heart: meshless model for cardiac mechanics, Biomech. Model. Mechanobiol. 18 (6) (2019) 1549–1561.
[71] Vahid Mohammadi, Mehdi Dehghan, Generalized moving least squares approximation for the solution of local and non-local models of cancer cell invasion of tissue under the effect of adhesion in one-and two-dimensional spaces, Comput. Biol. Med. 124 (2020), 103803.
[72] Hao Gao, Huiming Wang, Colin Berry, Xiaoyu Luo, Boyce E. Griffith, Quasi-static image-based immersed boundary-finite element model of left ventricle under diastolic loading, Int. J. Num. Methods Biomed. Eng. 30 (11) (2014) 1199–1222.
[73] Chi Zhang, Hao Gao, Xiangyu Hu, A Multi-Order Smoothed Particle Hydrodynamics Method for Cardiac Electromechanics with the Purkinje Network, 2021 *arXiv preprint arXiv:2110.02626*.
[74] Thomas Heidlauf, Röhrle Oliver, A multiscale chemo-electro-mechanical skeletal muscle model to analyze muscle contraction and force generation for different muscle fiber arrangements, Front. Physiol. 5 (2014) 498.
[75] S.A. Niederer, P.J. Hunter, N.P. Smith, A quantitative analysis of cardiac myocyte relaxation: a simulation study, Biophys. J. 90 (5) (2006) 1697–1722.
[76] R.H. Clayton, A.V. Panfilov, A guide to modelling cardiac electrical activity in anatomically detailed ventricles, Prog. Biophys. Mol. Biol. 96 (1–3) (January 2008) 19–43.
[77] R. Ruiz-Baier, A. Gizzi, S. Rossi, C. Cherubini, A. Laadhari, S. Filippi, A. Quarteroni, Mathematical modelling of active contraction in isolated cardiomyocytes, Math. Med. Biol. 31 (3) (September 2014) 259–283.
[78] Bertrand CW. Tanner, Thomas L. Daniel, Michael Regnier, Sarcomere lattice geometry influences cooperative myosin binding in muscle, PLoS Comput. Biol. 3 (7) (2007), e115.
[79] A. Fraticelli, R. Josephson, R. Danziger, Edward Lakatta, H. Spurgeon, Morphological and contractile characteristics of rat cardiac myocytes from maturation to senescence, Am. J. Physiol. Heart Circ. Physiol. 257 (1) (1989) H259–H265.
[80] Barış Cansız, Hüsnü Dal, Michael Kaliske, Computational cardiology: a modified hill model to describe the electro-visco-elasticity of the myocardium, Comput. Methods Appl. Mech. Eng. 315 (2017) 434–466.